Continuous antiretroviral therapy induces progressive senescence-like reprogramming of alveolar macrophages

Vinicius M. Fava,[1,2,*] Monica Dallmann-Sauer,[1,2,3] Marianna Orlova,[1,2] Wilian Correa-Macedo,[1,2,4] Ron Olivenstein,[5] Cecilia Theresa Costiniuk, [1,6,7] Jean-Pierre Routy,[1,6] Luis B. Barreiro,[8] and Erwin Schurr,[1,2,3]

[1] Program in Infectious Diseases and Immunity in Global Health, The Research Institute of the McGill University Health Centre; Montreal, QC, H4A 3J1, Canada.

[2] McGill International TB Centre, McGill University; Montreal, QC, H4A 3J1, Canada.

[3] Departments of Human Genetics and Medicine, Faculty of Medicine, McGill University, Montreal, QC, H3A 0C7, Canada.

[4] Present address. Canadian Centre for Computational Genomics (C3G) McGill University, Montreal, QC, H3A 0G1, Canada.

[5] Translational Research in Respiratory Diseases Program, The Research Institute of the McGill University Health Centre; Montreal, QC, H4A 3J1, Canada.

[6] Department of Medicine and Chronic Viral Illnesses Service, McGill University Health Centre; Montreal, QC, H4A 3J1, Canada.

[7] Graduate Program in Clinical and Translational Research, McGill University, Montreal, QC, Canada.

[8] Department of Medicine, Genetic Section, University of Chicago, Chicago, Illinois, IL 60637, USA.

* Corresponding author

Abstract

Background: Advances in antiretroviral therapy (ART) have substantially improved the lives of people with HIV (PWH) and reduced HIV acquisition through pre-exposure prophylaxis (PrEP). However, the long-term effect of ART on the physiological state of cells remains poorly understood. Despite the success of ART in preventing the progression of HIV infection to AIDS, aging PWH are suffering from a disproportional burden of non-AIDS comorbidities, including lung diseases.

Methods: Given the central function of alveolar macrophages (AM) in pulmonary immunity, we evaluated the impact of nucleoside reverse transcriptase inhibitors (NRTI) based ART on AM of PWH and people on PrEP. We employed a retrospective cross-sectional design and evaluated the effects of continuous exposure to ART in the epigenetic and transcript of AM at bulk and single-nucleus multiomics levels.

Results: We showed that continuous NRTI-based ART induces a progressive senescence-like pro-inflammatory state in AM, characterized by increased constitutive epigenetic and transcriptomic priming of genes involved in cell cycle arrest (e.g., *CDKN1A*/p21), components of the senescence-associated secretory phenotype (e.g., *IL1A*, *IL6R,* and *CXCL8*), as well as transcription factors subunits of the AP-1 family (e.g., *FOSL1, JUN*). At the AM single nucleus level we discovered a coordinated gene regulatory network linking key pro-inflammatory transcription factors to the transcriptomic alterations induced by ART. The senescence ART-linked epigenetic and transcriptomic changes were strongly dependent on the duration of ART and irrespective of HIV infection. A secondary time independent ART effect was observed for interferon signaling genes. This effect was more pronounced in people on PrEP and impaired the AM response to *ex vivo* challenge with SARS-CoV-2.

Conclusion: Combined, our data indicated that continuous NRTI-based ART promoted a dysregulated physiological state in AM, potentially contributing to age-related pulmonary comorbidities in PWH, such as COPD, pulmonary fibrosis, and asthma. The results of our study advocate for optimized or adjuvant therapies to mitigate potential long-term adverse effects of ART for people on PrEP and PWH.

47 **Background**

48 Advances in antiretroviral therapy (ART) have improved the quality of life for people with HIV
49 (PWH). In contrast to the initial regimens, current ART is more effective in the suppression of HIV and
50 has lower toxicity and adverse effects (1). In addition to treatment and health care improvements,
51 mitigation of opportunistic infections, and management of HIV comorbidities have greatly increased life
52 expectancy for PWH (2). Consequently, HIV infection is nowadays considered a chronic manageable
53 condition. The increased lifespan of PWH coincided with a surge of age-related idiopathic diseases
54 despite well-controlled HIV levels (3, 4), and the aging population of PWH now suffers a disproportional
55 burden of cardiovascular, neurological, and pulmonary diseases (5-7). The reasons for the increased
56 incidence of non-AIDS diseases in PWH remain poorly understood. HIV persistence, low levels of
57 inflammation and uncharacterized adverse effects of ART are among the potential contributors leading to
58 idiopathic diseases in PWH (8-12).

59 With respect to pulmonary involvement, PWH receiving ART exhibit increased susceptibility to
60 an array of pulmonary pathologies, including chronic obstructive pulmonary disease (COPD) (13),
61 mortality and severity due to COVID-19 (14, 15), tuberculosis (TB) (16, 17), pneumonia (18, 19),
62 pulmonary fibrosis (20), and lung cancers (21, 22). Central to the pathogenesis of these pulmonary
63 comorbidities are alveolar macrophages (AM) which are long-lived and self-renewing sentinel cells
64 within the lung microenvironment. We previously showed that AM isolated from PWH displayed an
65 attenuated epigenetic and transcriptomic response to *Mycobacterium tuberculosis* (*Mtb*), the etiological
66 agent of TB (17). Surprisingly, HIV-negative individuals receiving ART as pre-exposure prophylaxis
67 (PrEP) similarly exhibited attenuated AM responses to *Mtb*, implicating a direct pharmacologic effect of
68 ART independent of HIV status. Accordingly, we sought to delineate the impact of ART on the
69 epigenetic and transcriptomic landscape of AMs in both PWH and persons receiving PrEP. We found that
70 exposure to ART significantly altered the epigenetic and transcriptomic state of AM, imprinting a
71 progressive, duration-dependent senescence-like phenotype and a disruption of constitutive interferon

72 signaling. To further characterize the effects of ART on AM heterogeneity, we employed a single-nucleus
73 multiomics (snMulti) approach to assess AM responses following SARS-CoV-2 challenge. These
74 experiments revealed that ART modulates the composition of AM subpopulations and substantially
75 diminishes AM *ex vivo* reactivity toward SARS-CoV-2.

76 **Methods**

77 *Subjects and study design*

78 To study the impact of ART on the AM physiological state, we used both bulk and snMulti
79 approaches (**Fig. 1**). Subjects included in the bulk section of this study were enrolled as part of our study
80 on AM responses to *Mtb*. Hence, details of quality control regarding Bronchoalveolar Lavages (BAL)
81 practice, AM processing and preparation were as described previously (17). We excluded subjects with
82 previous pulmonary infections, abnormalities in baseline lung functions, pulmonary conditions, chronic
83 cardiovascular or metabolic diseases and illegal substances abuse. In addition, we applied the following
84 technical exclusion criteria for the bulk approach: samples with fraction of reads in peaks < 10% and
85 libraries with less than 20 million reads. Of the 42 subjects that passed quality control, 14 were healthy
86 HIV-negative without ART (HC); 10 were HIV-negative at a high exposure setting for HIV under PrEP;
87 and 18 were PWH under ART (**Table 1**). Participants had uninterrupted use of ART ranging from two
88 months to 5.4 years for PrEP and from seven months to 23.1 years for PWH at the time of BAL cell
89 collection. None of the participants had developed resistance to ART and all regimens included at least
90 one NRTI. Due to the limited yield of AM from BAL some bulk assays could not be tested in all subjects
91 (**Table 1**). For the snMulti approach we enrolled 3 PrEP and 3 PHW participants on long term ART, and
92 3 HC for BAL recollection (**Table 1**). However, one HC sample failed library preparation and was
93 excluded.

94 To assess the epigenetic and transcriptomic state of AM we used five different assays (**Fig. 1a**).
95 We tested the hypothesis that ART imprinted a physiological state in AM that primed pathways linked to
96 pulmonary diseases. We carried out the bulk testing in three separate steps (**Fig. 1b**). (i) We compared the

97 epigenetic and transcriptomic state of AM between the HC, PrEP and PWH groups independent of time
98 on ART. (ii) We tested the effect of time on ART in PrEP and PWH individuals separately. Accessibility
99 of chromatin regions, histone marks, and gene expression changes with increased time for both groups
100 were denoted as having an ART effect. (iii) We conditioned the effect of continuous exposure to ART on
101 the PrEP/PWH/HC group status to highlight the main biological mechanisms affected by continuous
102 exposure to ART. Next, we employed snMulti to assess AM subpopulation specific effects on models (i)
103 and (iii); and (iv) to evaluate group differences to SARS-CoV-2 challenge, which we used as an
104 experimental probe for the AM immune response (**Fig. 1b**).

105 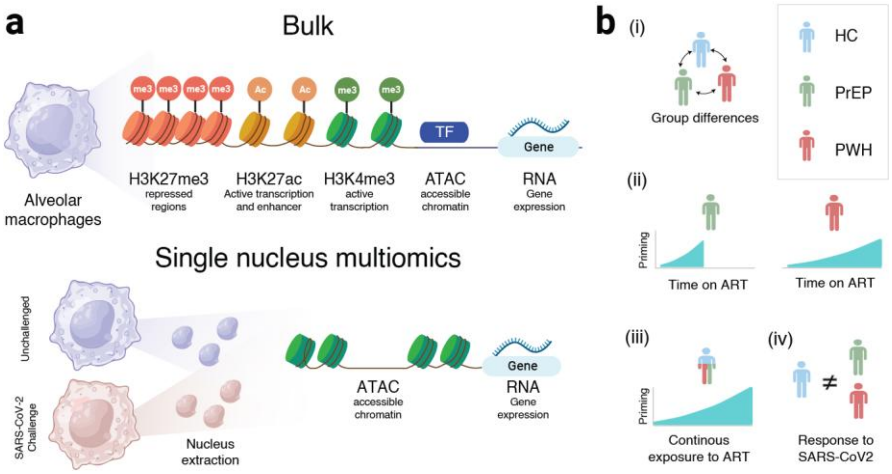

106 **Fig. 1. Study design overview.**

107 (**a**) Assays used to evaluate the physiological state of alveolar macrophages at bulk and single nucleus
108 level. (**b**) Models tested to assess the biological mechanisms affected by ART in alveolar macrophages:
109 (i) Differences between groups independent of duration of time on ART; (ii) The effect of time on ART
110 for PrEP and PWH participants; (iii) Continuous exposure to ART while accounting for group status, (iv)
111 Group specific difference in response to SARS-CoV2 challenge. (Created with BioRender).

112 *Bronchoalveolar lavages*

113 Bronchoscopies were performed at the Centre for Innovative Medicine of the MUHC as per
114 American Thoracic Society guidelines and as previously described (17, 23). Briefly, standard flexible

115 bronchoscopy of the middle lobe was conducted under local anesthesia with lidocaine with additional
116 conscious sedation with intravenous midazolam. A total of 200 ml sterile saline instilled in 50-ml
117 volumes resulted in an average return of 115 ml of BAL fluid. BAL fluid in non-adherent tubes was
118 stored on ice for a maximum of 30 minutes. Prior to further processing, BAL fluids were strained through
119 100µm filter to remove any mucus and cell clumps. Cytology assessment was performed for all BAL
120 samples and indicated that AMs represented >85% of all recovered mononuclear cells. Collected BAL
121 cells were spun for 10 minutes at 300g, 10°C, and washed twice in RPMI-1640 with L-glutamine
122 (Wisent, Canada), containing 2.5% human serum (heat-inactivated AB+ off the clot, Wisent, Canada), 1%
123 penicillin/streptomycin (Gibco, USA), 10mM HEPES (Gibco, USA), 1% non-essential amino acids
124 (Gibco, USA) and 2.5 µg/ml Amphotericin B (Wisent, Canada). BAL cells were counted and seeded at
125 ~250K cells/well in low attachment 24-well plates (Nunclone Sphera®) for culture and viral infection.

126 *Library preparation*

127 Data for bulk RNAseq, ATACseq, and H3K27ac was generated previously and the methodology
128 used to prepare libraries and to process the data for RNA-, ATAC- and H3K27ac was described in (17).
129 For this study, we added two histone marks: H3K4me3 and H3K27me3. We also expanded the dataset for
130 the H3K27ac mark. Libraries for the three histone marks were produced using ChIPmentation kits for
131 histones from Diagenode (C010110009). Aliquots of crosslinked AM containing 10^5 cells stored at -80°C
132 were thawed and resuspended on 50 µL of ice-cold Sarkosyl buffer. Next, samples were sonicated on
133 Bioruptor Pico to obtain fragments between 200 – 500 bp. ChIPmentation was carried out using the
134 automated IP-Star Compact with Diagenode recommended protocol and the Diagenode antibodies for
135 H3K4me3 (C15410003), H3K27ac (C15410196), and H3K27me3 (C15410195). After overnight
136 incubation, DNA fragments captured by the immunoprecipitation were reverse crosslinked and unique
137 barcodes, Diagenode (C01011034, C01011036, and C01011037), were added to the sequences of each
138 subject and histone mark. Finally, libraries were sequenced on Illumina NovaSeq 6000 S4 PE100 aiming

139 for an average of 50 million reads per library. The raw sequences were then processed using the same
140 protocol previously reported (17).

141 For the snMulti, nuclei preparation was done following an adapted 10xGenomics protocol
142 (CG000365). Specifically, to obtain good quality AM nuclei from BAL cells were lysed while beating with
143 3mm glass beads for 4 second on MP Biomedicals™ FastPrep-24™ (speed 6.5). Next, ATAC and gene
144 expression libraries were constructed following manufacturer's instructions using 10xGenomics Epi
145 multiome ATAC + Gene Expression kit (CG000338). snMulti libraries were paired-end sequenced on
146 Illumina NovaSeq 6000 S4 flow cells.

147 *snMulti quality control and data integration*

148 Single-nucleus multimodal sequencing data was processed using 10X cellranger-arc v.2.0.2 with
149 default parameters. Barcoded reads from each single nucleus were aligned to the human genome
150 GRCh38. Data processing was performed per modality prior to multimodal integration. First, HDF5 files
151 with gene expression count were imported into R using BPCells v.0.3.0 (24) and processed with Seurat
152 v5.2.1 (25). Nucleus with mitochondrial reads > 0.2 and detectable genes < 300 were excluded. Next,
153 chromatin accessibility counts and fragments for nucleus that passed quality-control for the RNA
154 modality were imported to Seurat and processed using Signac v.1.14.0 (26). We used a unified peak set
155 across all samples to recalculate feature matrix counts before snATAC integration. We then estimated
156 snATAC parameters and excluded nucleus with fraction of reads in peaks < 0.6, nucleosome signal < 1.5,
157 TSS enrichment < 1, and counts < 1000.

158 The snRNA modality was integrated using the standard Seurat multiomics pipeline. The data for
159 each library was normalized with SCTransform, and integration was performed using *IntegrateLayers*
160 with reciprocal PCA (RPCA) using one unchallenged library from each group (HC, PrEP, and PWH) as a
161 reference and the top 30 PCs. Dimensionality reduction and clustering were performed using
162 *FindNeighbors, FindClusters*, and *RunUMAP*, to define cells subpopulations and to separate AM from
163 DCs and lymphocytes, which represented between 0.1% and 10% of total cells from BAL. snATAC

164 integration followed Signac pipeline. Term frequency–inverse document frequency (TF-IDF)
165 normalization was applied, followed by latent semantic indexing (LSI) via *RunSVD*. The LSI 2 to 15 were
166 used for dimension reduction and clustering. The first LSI component was excluded from the integration
167 as it captures sequencing depth. Cell subpopulations were identified using the same approach as for the
168 snRNA modality. Finally, we performed weighted nearest neighbor (WNN) analysis using Seurat
169 *FindMultiModalNeighbors* to integrate the RPCA and LSI reductions from snRNA and snATAC,
170 respectively. snMulti WNN clusters were used to define the AM subpopulations shown throughout the
171 manuscript.

172 *Single nucleus annotation*

173 To identify the main biological processes characterizing the physiological state of AM
174 subpopulations we used Seurat *FindConservedMarkers* for unchallenged, and SARS-CoV-2 challenged
175 libraries separately. Next, we used cluster markers with positive fold changes expressed in > 25% of the
176 unchallenged AM for each subpopulation to perform a gene ontology (GO) analysis using *enrichGO* form
177 clusterProfiler (27). We selected the most significant GO term per subpopulation as a proxy of the main
178 physiological state of the AM clusters. We then calculated a module score using *AddModuleScore* using
179 the cluster marker genes per nucleus for the top GO terms and indicated the density of the biological state
180 in the UMAP using *plot_density* from Nebulosa v.1.0.1 (28). To identify a transitional state of the AM
181 subpopulations we performed pseudotime and trajectory analysis using unchallenged libraries with
182 slingshot v.2.14.0 (29).

183 *snMulti SARS-CoV-2 ex vivo challenge*

184 We used the SARS-CoV-2 strain RIM-1 isolated from a patient in Quebec (GenBank ID
185 MW5997360) (30). The SARS-CoV-2 strain was propagated using VeroE6 cells infected at a multiplicity
186 of infection (MOI) of 0.05 TCID50/cell and incubated in DMEM at 37 °C for 3 days. The virus-
187 containing supernatant was harvested, clarified by centrifugation at 2,000g for 5 min. Cell-associated
188 viruses were obtained by 3 freeze/thaw cycles, where cell debris was removed by centrifugation at

189 4,000g. Viral stocks were concentrated using Amicon® Ultra-15 100K Centrifugal Filter Units. BAL
190 cells were *ex vivo* challenged with SARS-Cov2 at MOI 2:1 TCID50/cell or left untreated overnight (16-
191 18 hours) in culture medium RPMI (Gibco) with 2.5% human serum, 1% penicillin/streptomycin, 10mM
192 HEPES, 1% non-essential amino acids and 2.5 µg/ml Amphotericin B. Further, cells were collected by
193 gentle pipetting, washed twice in PBS (Wisent), 0.04% BSA (Wisent) and 20 µg/ml DNase I (Roche) to
194 prevent cell clumping and assessed for viability.

195 *Statistical modeling*

196 Bulk differences in epigenetics and transcriptomics of AM were tested with three models
197 comparing: (i) groups: PrEP, PWH and HC; (ii) time on ART for PrEP and for PWH, and (iii) continuous
198 exposure to ART adjusted by group with the following linear modeling in Limma v3.60.2 (31):

199 (i) $$Y_{(i,j)} \sim \beta 0_{(i)} + \beta_{Groups} \cdot X_{Groups\ (PrEP,PWH)} + \beta_{Confounders} \cdot X_{(Confounders)} + \beta_{Batches} \cdot X_{(Batches)} + \varepsilon_{(i,j)}$$

200 (ii) $$Y_{(i,j)} \sim \beta 0_{(i)} + \beta_{Time \times Groups} \cdot (X_{Groups\ (PrEP,PWH)} \times X_{Time}) + \beta_{Groups} \cdot X_{Groups\ (HC,PrEP,PWH)}$$

201 $$+ \beta_{Confounders} \cdot X_{(Confounders)} + \beta_{Batches} \cdot X_{(Batches)} + \varepsilon_{(i,j)}$$

202 (iii) $$Y_{(i,j)} \sim \beta 0_{(i)} + \beta_{Time} \cdot X_{Time} + \beta_{Group} \cdot X_{Groups\ (HC,PrEP,PWH)} + \beta_{Confounders} \cdot X_{(Confounders)} + \beta_{Batches} \cdot X_{(Batches)} + \varepsilon_{(i,j)}$$

203 Where $Y_{(i,j)}$ represents the estimate quantification for each feature "i" and sample "j". Briefly,
204 quantification matrices with $Y_{(i,j)}$ were depth-normalized with *calcNormFactors* upperquartile (0.75) for
205 the epigenetic assays and TMM for the transcriptomic data using edgeR v.3.40.2. The mean-variance
206 relationship and log2 count per million was estimated with *voom* v3.60.2 (32). In these models, $\beta 0_{(i)}$
207 represents the intercept for the feature "i". In model (i) the intercept corresponds to the HC group. In
208 models (ii) and (iii) the intercept represents the predicted value of Y when the continuous variables of
209 interest (e.g. Time on ART) are equal to zero. In model (i) β_{Groups} output two β that captures the main
210 effect for PrEP and PWH relative to the intercept (HC), respectively. The contrast between PrEP and
211 PWH was done post-hoc by contrasting their respective β coefficients. In models (ii) and (iii) the β_{Groups}
212 adjusts for the main effect of group membership on the "Time" effect. In model (ii) the $\beta_{Time \times Groups}$ is an
213 interaction term that output two β that captures the effect of time on ART for PrEP and for PWH. In

214 model (iii) the β_{Time} term estimates the effect of continuous exposure to ART adjusting for the main group
215 effect. The coefficients of $\beta_{Confounders}$ included the phenotypic confounders: sex, chronological age,
216 smoking status, *Mtb* challenge, and a seasonal effect of BAL collection. The coefficients of $\beta_{Batches}$
217 included the technical covariates: sequencing batch, fractions of reads in peaks for the epigenetic assays,
218 time of AM incubation, and number of AM seeded per plate. The $\varepsilon_{(i,j)}$ represents the residual error not
219 explained by variables in the model. A Benjamini–Hochberg (BH) procedure was used to estimate False
220 Discovery Rate (FDR) for each assay in the three tested models. Genes and peaks presenting FDR < 10%
221 were selected for further follow-up on the pathway and transcription factors analyses.

222 snMulti differential analysis was performed using a pseudo bulk approach per AM
223 subpopulations. Briefly, pseudo counts per AM subpopulations, subject, and challenge status were
224 calculated using Seurat *AggregateExpression*. Next, genes expressed in less than 20% of the nuclei of a
225 subpopulation for the snRNA modality and peaks quantified in less than 5% of the snATAC modality
226 were excluded from the analysis. For the snATAC pseudo bulk we filtered for peaks linked to genes.
227 Chromatin region from snATAC were assigned to genes using Signac *LinkPeaks*. Peaks that correlated
228 with flanking gene expression within 250kb with a Pearson correlation > 0.01 and *p* value < 0.1 were
229 selected for downstream analysis. We used this lenient cut off to avoid removing epigenetic features that
230 lacked stronger correlations with genes due to the sparsity of the snATAC data. The pseudo counts per
231 modality was performed as in bulk (32, 33). The statistical analyses testing differences between groups
232 and continuous exposure to ART applied the same statistical framework of models (i) and (iii). To test
233 AM response to SARS-CoV-2 challenge per group we used a per subject paired design as indicated in the
234 equation below.

235 (iv) $$Y_{(i,j)} \sim \beta 0_{(i)} + \beta_{(\text{Groups (HC, PrEP, PWH)} \times \text{Challenge})} \cdot X_{(\text{Groups (HC, PrEP, PWH)}} \times X_{\text{Challenge})} + \beta_{\text{Time} \times \text{Challenge}} \cdot$$
236 $$(X_{\text{Time}} \times X_{\text{Challenge}}) + \beta_{(\text{Subjects})} \cdot X_{(\text{Subjects})} + \varepsilon_{(i,j)}$$

237 In this model, $\beta 0_{(i)}$ represents the intercept which corresponds to one unchallenged HC library followed
238 by two interaction terms. The first interaction term captures the effect of SARS-CoV-2 challenge with one

239 output β per Group (HC, PrEP, and PWH) and the second interaction term β captures the effect of SARS-
240 CoV-2 according to the time of continuous exposure to ART. Then one β per subject characterizes the
241 blocking design and the $\varepsilon_{(i,j)}$ represents the residual error not explained by variables in the model.

242 *Bulk peak to gene assignment and Gene-Set Co-Regulation Analysis*

243 Genes were assigned to peaks using *annotatePeak* from ChIPSeeker v.1.40 (34). Each peak from
244 the epigenetic assays was assigned to the nearest gene and to any additional flanking gene at < 5 kilobases
245 from a peak. The gene set co-regulation analysis (GESECA) was performed with *geseca* from *fgsea* v1.30
246 (35). Briefly, GESECA identifies patterns of co-expression, co-accessibility or co-marks enriched within
247 predefined gene sets across samples. GESECA was developed to compare datasets with a large number of
248 different biological conditions such as timepoints (e.g. time on ART). It uses as input a quantification or a
249 covariate-reduced matrix (gene/peak by samples) to calculate the proportion of variance between samples
250 explained by each gene set. *P*-value significance for each gene set is then calculated by permutation of
251 genes between lists. For the GESECA we used covariate-regressed matrices obtained via
252 *removeBatchEffect* from *Limma* for transcriptome and epigenome. By design, GESECA does not directly
253 compare phenotypic groups but rather variability between samples (i.e., individuals GESECA scores). To
254 assess if the variability between samples was driven by group or a time effect, we contrasted the
255 GESECA score per subject with the phenotype of interest in each model. For group comparisons, we used
256 a Wilcoxon test to estimate significant differences between the median GESECA score per group. To test
257 the correlation of time and GESECA scores we used linear regression both for the per-group time
258 comparisons (PrEP and PWH) and the overall effect of continuous exposure to ART. An FDR correction
259 for these comparisons was calculated using BH. We ran GESECA using the HALLMARK pathway gene-
260 set collection from MSigDB (36). Additionally, as senescence is a hypothesized mechanism contributing
261 to comorbidities in the aging PWH we included the REACTOME "Senescence" branch, and SenMayo, a
262 well-established senescence gene set across tissues and species in the gene-set lists (37, 38).
263

264 *Motif enrichment analysis*

265 To test for enrichment of transcription factor binding motifs in differential regions associated
266 with the continuous exposure to ART, we used *findMotifsGenome* from HOMER v4.11 (39). Differential
267 accessible chromatin regions (ATAC) were compared to (i) 500,000 random regions matched by size and
268 GC content and (ii) nonsignificant 20,060 regions at FDR > 50% in the continuous exposure to ART
269 analysis. We considered a motif to be significantly enriched if it presented FDR < 1%. Pairwise
270 correlation of TF motif binding by similarities was performed with STAMP v.1.3 default parameters (40).

271 *Footprint analysis*

272 Transcription factor Occupancy also known as Footprint analysis was performed with TOBIAS
273 v0.14.0 using covariate-regressed ATAC traces (41). Briefly, we adapted the concept of regressing out
274 known confounders (e.g. covariables and batch effects) prior to chromatin modeling as proposed in (42,
275 43). First, signal intensity for regions with increased chromatin accessibility (ATAC) with continuous
276 exposure to ART was calculated from BAM files of each subject using *bamCoverage* from deepTools
277 v.3.5.1 with --binSize 1 and --normalizeUsing CPM (44). Next, ATAC signals per sample were
278 summarized using *multiBigwigSummary* (44). The output of this procedure was a quantification matrix
279 with ATAC signal intensity at 1bp resolution per subject. This matrix was then exported into R v4.4.0.
280 We used *removeBatchEffect* from *Limma* to calculate the residual signal intensity after regressing the
281 coefficients $\beta_{\text{Group (HC,PrEP,PWH)}}$, $\beta_{\text{Confounders}}$ and β_{Batch} while preserving β_0 and $\beta_{Time.}$ from the model (iii). This
282 residual signal intensity matrix represents ATAC traces mimicking the linear model (iii) tested in the
283 differential analysis. The residual traces were exported from R and converted back to individual BigWigs
284 using *bedGraphToBigWig* from UCSC. Next, we used TOBIAS *ScoreBigwig* to identify regions of
285 protein binding across differential regions with continuous exposure to ART. To predict which TF bind to
286 the footprints detected, we combined footprint scores per subject with information on TF binding motifs
287 using TOBIAS *BINDetect*. We used as reference 919 motifs from the JASPAR CORE database for
288 vertebrates (45). *BINDetect* calculates a mean footprint score for each of the 919 TF binding sites split per

289 subject. This score can be compared between samples to access differential changes as TF having high-
290 scoring footprints denotes a clearer and more defined bound. To test if the TF footprint intensity was
291 associated with time, we fit a linear model comparing the footprint mean intensity per TF with the
292 continuous exposure to ART. Fold change per year was calculated via the exponential of the model slopes
293 and FDR *p*-values were adjusted with BH. TOBIAS *PlotAggregate* was used to summarize traces for
294 selected examples of TF. The residual signal intensities for selected examples of footprints were plotted
295 per timepoint and according to their chromosomal position for each assay using *ggplot2* v.3.4.4 with
296 *geom_spline* from *ggformula* v.0.10.4 (46, 47).

297 *snMulti transcription factor signature and gene regulatory network*

298 We infer TF activity signature using decoupleR v2.4.1 as previously described (48, 49). Briefly,
299 TF – target gene interaction network was obtained from the collecTRI database. We filtered the snRNA
300 modality for genes significantly associated with continuous exposure to ART (FDR < 10%) within the
301 AM subpopulation. TF activity scores were computed per cell using *run_ulm*, which
302 fits a linear model that predicts the observed gene expression based solely on the TF-Gene interaction
303 weights, with the t-value of the slope used as the activity score. To evaluate the relationship between TF
304 activity and continuous exposure to ART, we modeled TF scores as a function of time, adjusting for
305 group (HC, PrEP, PWH) using the *lm* function in base R. β coefficients representing the effect of
306 continuous exposure to ART on TF activity were extracted, and a BH FDR was calculated. TFs showing
307 absolute $\beta > 0.02$ and FDR < 0.01 were considered significant.

308 To infer the multimodal TF gene regulatory networks (GRN) associated with continuous
309 exposure to ART, we applied the Pando v1.0.2 framework (50). Pando models gene expression as a
310 function of the interaction between TF expression and chromatin accessibility at regions with TF binding
311 sites per nucleus. For the GRN analysis, we tested 627 TFs from the JASPAR2020 human CORE
312 collection (51). As candidates for the GRN, we evaluated all differential features for snRNA (n = 867)
313 and snATAC (n = 3,332) associated with continuous exposure to ART. Regulatory TF interactions were

314 modeled with *infer_grn* using the Signac peak-to-gene method, a 250 kb upstream and 50 kb downstream
315 window, and multiple testing correction using the BH procedure. Modules of co-regulated genes were
316 identified using *find_modules*, and modules with FDR < 10% were considered significant.

317 **Results**

318 *Differences in AM physiology between PWH, people on PrEP and HC*

319 To assess the correlation of epigenetic and transcriptomic features (i.e., accessible chromatin,
320 H3K27me3, H3K27ac, H3K4me3, and RNA) with study group we performed a principal component
321 analysis (PCA). After accounting for known confounders (smoking, sex, chronological age, and batch)
322 and preserving the phenotype group variable, the top four principal components (PC) captured between
323 38% to 75% of the remaining variability. Yet, the top components only partially clustered subjects
324 according to their respective groups suggesting strong interindividual variability (**Fig. 2a**). As a result,
325 when performing the differential feature analysis, only a small proportion of the regions tested passed
326 with FDR < 10% while differences in gene expression were more pronounced (**Fig. S1; Table S1**).
327 Among genes with decreased expression in PrEP, we identified all 13 mitochondrial-encoded genes of the
328 electron transport chain (**Fig. S2**). This indicated a potential mitochondrial dysfunction in AM from PrEP
329 that was also observed to a lesser extent for PWH.

330 Given the pronounced interindividual variability across all studied groups, we performed a
331 GESECA to identify pathways associated with the most highly variable features (see methods). Using this
332 approach, we found that differences between subjects were significantly enriched in inflammatory,
333 cellular homeostasis and stress related pathways both at the transcriptomic and epigenetic levels (**Fig. 2b;**
334 **Table S2**). Next, we evaluated if the differential pathways between subjects were driven by the
335 phenotypic groups (**Fig. 2c**). We found that genes assigned to the DNA repair pathway had significantly
336 increased expression in AM from PWH compared to PrEP and HC. DNA repair is a known mechanism
337 activated in host response to HIV integration. In contrast, expression of genes assigned to interferon
338 pathways were significantly depleted in AM from PrEP and PWH compared to HC (**Fig. 2c**). Of the 183

genes of hallmark interferon pathways that are expressed in AM, 28 (15.3%) had decreased expression in PrEP compared to HC with most of these genes displaying a trend of decreased expression in PWH (**Fig. 2d**). Among key genes with lower expression in PrEP were Interferon-Inducible genes (IFIs), Interferon Regulatory Factors (IRFs), and interferon receptors both type-I (*IFNAR2*) and type-II (*IFNGR1*) (**Fig. 2e; Table S1**).

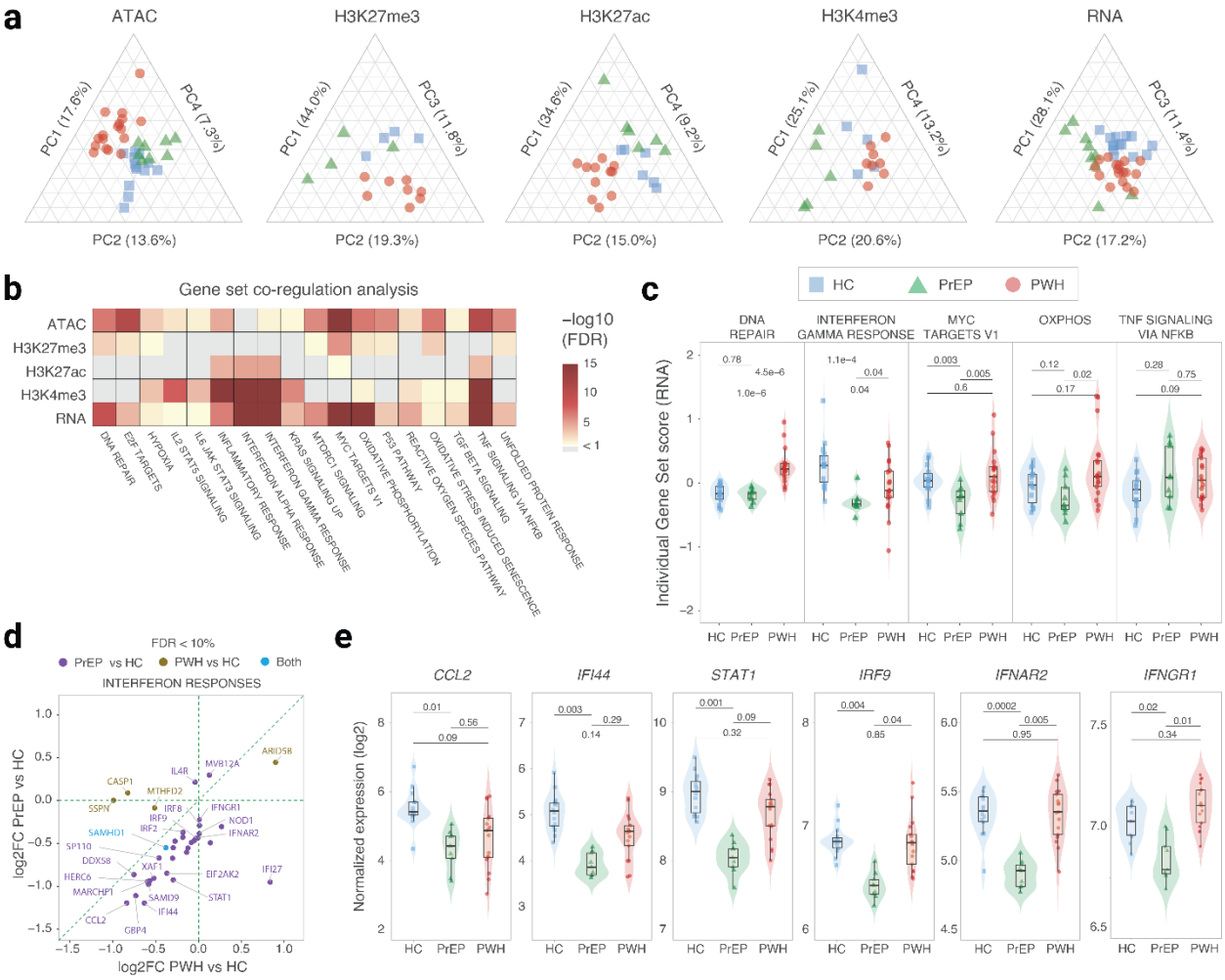

Fig. 2. Epigenetic and transcriptomic differences between AM from people on PrEP, PWH and HC.

(a) Phenotypic group clustering using the top principal components (PCs). Scaled PCs and their corresponding percentage of variance explained are shown on each axis of the ternary plots for the five tested assays. **(b)** Gene Set Co-regulation Analysis (GESECA) for Hallmark pathways. Gene sets with False Discovery Rate (FDR) < 10% in at least three assays. Results for all tested pathways are given in

350 Table S2. (**c**) GESECA scores for the top five differential pathways. The scores of the transcriptomic
351 assay for each subject are indicated on the y-axis separated by group on the x axis. (**d**) Correlation
352 between differential expression for interferon response genes in PrEP and PWH versus HC. The log2 fold
353 difference (log2FC) between PrEP and HC was plotted against the log2FC for PWH vs HC for the
354 transcriptomic assay. Each circle represents a gene in the Hallmark interferon pathways that had FDR <
355 10%. **(e)** Normalized gene expression per subject and group for selected genes in HALLMARK interferon
356 pathways. In panels "c" and "e", a Wilcoxon test was used to estimate significant differences in the
357 median between groups with the FDR adjusted *p*-values shown at the top for each group comparison.

358

359 Overall, the group comparison indicated an active DNA damage repair (DDR) mechanism in AM
360 from PWH and a constitutive lower expression of interferon-related genes in AM that was more
361 pronounced in PrEP participants. On the other hand, the inter-individual variabilities associated with TNF
362 signaling pathways were not captured by group assignment (**Fig. 2c**). The lack of association between
363 gene set scores for these pathways and group labels suggested that unaccounted participant characteristics
364 were likely driving the inter-individual variability. However, when displaying the time of continuous
365 exposure to ART for the individuals in Fig. 2c we observed a strong trend for a time dependent effect on
366 TNF signaling for AM from both PrEP and PWH (**Fig. S3**). We therefore hypothesized that time on ART
367 for PrEP and for PWH is an important factor to explain differences in AM state between subjects.

368 *The effect of time on ART on the transcriptomic and epigenetic landscape of AM*

369 While accounting for the same covariates as in the previous analyses, we added a time variable to
370 the model and tested PrEP and PWH groups independently. The time variable captured the fraction of
371 years from the start of the ART regimen to BAL collection (**Table 1**). To avoid regressing out the
372 variable of interest, we conducted a PCA on the residuals after removing confounders and preserving the
373 time variable. With this approach we showed that PC1 strongly correlated with time on ART in both PrEP
374 and PWH in all tested assays (**Fig. 3a**). We observed a high proportion of significant differential

375 epigenetic and transcriptomic features at FDR < 10% for time on ART for PrEP and length of time since
376 ART initiation for PWH (**Fig. 3b; Table S3**). Chromatin accessibility and the H3K27ac mark showed the
377 highest numbers of significantly differential features affected by time in both groups. Additionally, PWH
378 presented >5-fold more time-dependent differentially expressed genes compared to the PrEP participants
379 and more active promoters with increased H3K4me3 (**Fig. 3b; Table S3**). This may reflect HIV-specific
380 effects, time-dependent changes not detected in the PrEP group due to the shorter ART regimen, or higher
381 statistical power due to the larger sample size of the PWH group. To compare features affected by time on
382 ART in both groups, we intersected genes and features significantly associated with time in the PrEP and
383 PWH groups (**Fig. 3c**). With the exception of the promoter repressor H3K4me3 mark, we identified a
384 significant enrichment of changes occurring in the same direction for time on ART in both PrEP and
385 PWH groups (**Fig. 3c**).

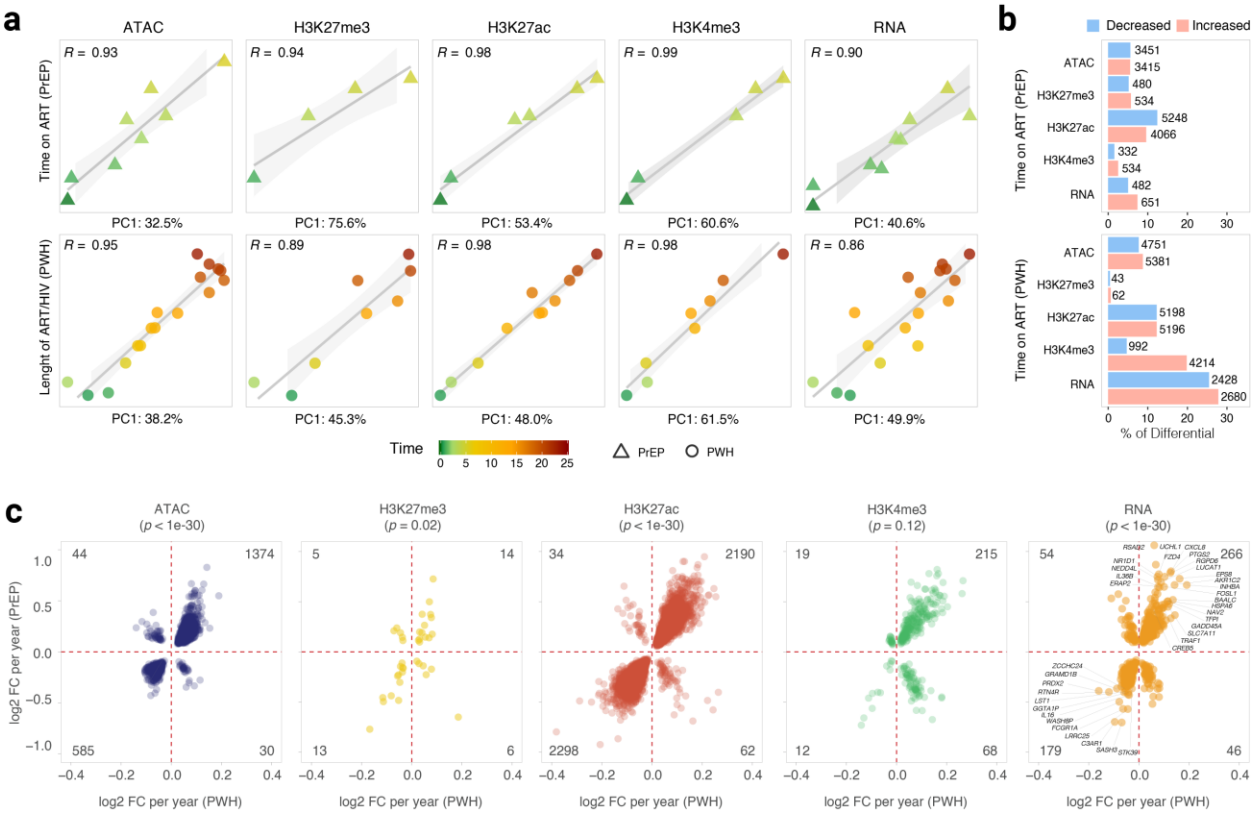

386

387 **Fig. 3. Differential epigenetic and transcriptomic features with time on ART for PrEP and PWH.**

388 (**a**) The proportion of variance captured by the first principal components was plotted against time on
389 ART for people on PrEP (top) and for PWH (bottom). The Pearson correlation R is shown at the left
390 upper corner of each plot. (**b**) Epigenetic and transcriptomic features significantly associated with time on
391 ART in PrEP and PWH participants. The bar plots show the proportion of differential regions/genes at an
392 FDR of 10% relative to the total number of tested regions/genes for time on ART in PrEP (top) and in
393 PWH (bottom). The absolute numbers of differential regions/genes are shown next to the bars. Decreased
394 and increased DNA accessibility, histone marks, and gene expressions are shown in blue and red,
395 respectively. (**c**) Epigenetic and transcriptomic features significantly changed in the same direction with
396 time for PrEP and PWH participants. Only features with FDR < 10% in both groups are plotted
397

398 *Biological mechanisms affected by time on ART in PrEP and PWH*

399 To assess the biological mechanisms affected by time on ART we performed a GESECA analysis
400 separately for the PrEP and PWH groups (**Table S2**). We highlighted 15 gene sets with the highest
401 variability between samples within the PrEP and PWH groups (**Fig. 4a**). These terms included OXPHOS,
402 immune mediators, control of cellular stress, cell cycle arrest, and senescence (**Fig. 4a**). Next, we tested if
403 the per individual GESECA score of highlighted pathways correlated with time on ART in PrEP and
404 PWH (**Fig. 4b; Fig. S4**). At the RNA level, 14 out of 15 pathways significantly correlated with time in at
405 least one group ($P \leq 0.01$) (**Fig. 4b; Fig. S4**). At the epigenetic level, time on ART correlated ($P \leq 0.01$)
406 with individual GESECA scores in all highlighted pathways for at least one active epigenetic assay
407 (ATAC, H3K27ac, and H3K4me3). Decreased expression of genes assigned to the OXPHOS pathway
408 correlated with time on ART in PWH, but not in the PrEP group (**Fig. 4b**). However, hallmark OXPHOS
409 pathway do not encompass mitochondrial genes of the electron transport chain that had decreased gene
410 expression in PrEP and PWH independent of time on ART (**Fig. S2**). This suggested that time on ART
411 may impact different components of OXPHOS at different levels. This is supported by the decreased

412 expression of autosomal genes encoding members of the electron transport chain complexes I–V that was
413 more pronounced with increased time on ART in PWH (**Fig. 4c**).
414 Transcription of genes assigned to the TNF signaling pathway correlated with time on ART in
415 both the PrEP and PWH groups (**Fig. 4b**). The increase in the transcription-based GESECA score per year
416 for the TNF pathway was higher in PrEP compared to PWH (**Fig. 4b**). Among the genes assigned to TNF
417 signaling that displayed increased expression with time on ART were transcription factors that are key
418 mediators of immune responses and senescence (**Fig. 4c**). For example, subunits of the AP-1 complex
419 (e.g. *JUN* and *FOSL1*), and AP-1 cooperative regulators (e.g. *EGR1*, *ATF3*, *ETS2,* and *KLF10*) had
420 increased expression with time on ART in AM from subjects on PrEP and PWH (**Fig. 4c**). Moreover, key
421 pro-inflammatory mediators such as *PTGS2* (i.e. COX-2) and *TNF* showed increased expression with
422 time on ART in both groups, albeit *TNF per se* did not surpass FDR correction (**Fig. 4c**). For these key
423 genes we also identified a time-related effect at the epigenetic level. For example, the transcription
424 starting site (TSS) of *FOSL1* and *PTGS2* had increased chromatin accessibility, as well as H3K27ac and
425 H3K4me3 marks with increased time on ART (**Fig. 4d**).

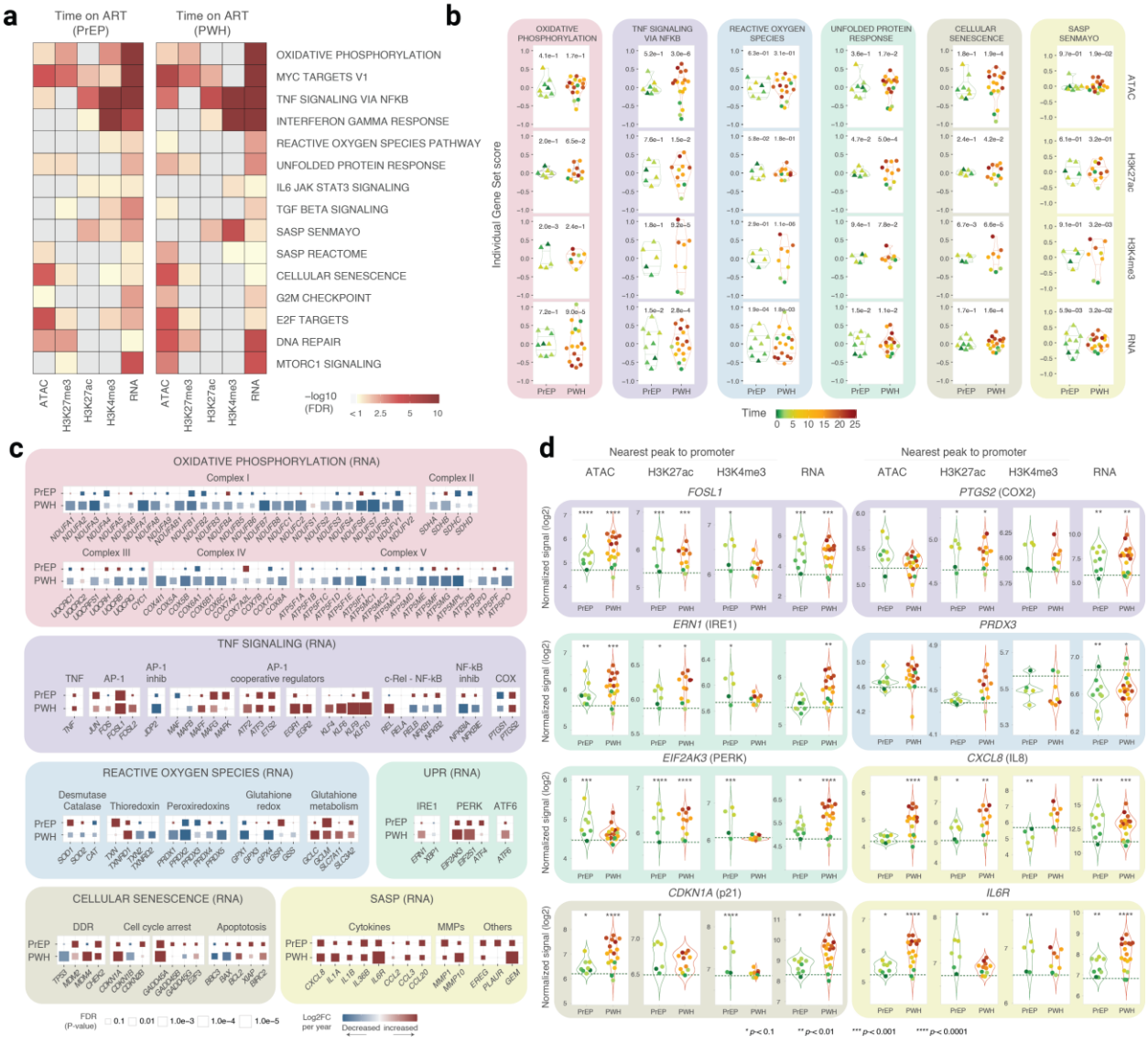

426

427 **Fig. 4. Biological pathways affected by time on ART in people on PrEP and in PWH.**

428 (**a**) GESECA gene sets with the largest variability between participants within each group. Terms with
429 FDR < 10% in at least two assays in each group are shown as a heatmap. Data for all tested gene sets is
430 given in Table S2. (**b**) Per subject GESECA scores (y-axis), separated by group (x-axis) for six gene sets
431 affected by time on ART. Remaining pathways are shown in Fig. S4. The quantiles are shown as violins
432 for reference of the distribution. A linear model was used to test the correlation of time on ART in PrEP
433 and PWH with the individual GESECA scores for all tested assays. *p*-values for the correlations are
434 shown at the top of each comparison. The repressor mark H3K27me3 did not show a significant

435 correlation with time in any group and was omitted. (**c**) Changes in gene expression for selected genes
436 belonging to pathways shown in panel "b". Genes were grouped by main function in each pathway. The
437 absolute values for log2FC and FDR are shown in Table S3. (**d**) Promoter accessibility and histone
438 marks, and expression of selected genes affected by time on ART in both groups. A dotted horizontal
439 green line indicates the average signal in healthy controls for reference. *p*-values are given at the top of
440 the group for each comparison with the absolute values and FDR shown in Table S4.

441

442 Time on ART also impacted on the AM cellular response to stress via inactivation of reactive
443 oxygen species (ROS) and protein turnover via the unfolded protein response (UPR) (**Fig. 4b**). For the
444 ROS pathway we noted a distinct effect of time for AM from the PrEP and PWH groups at the RNA level
445 (**Fig. 4b**). However, this was due to groups capturing different aspects of the ROS pathway. For example,
446 redoxins (e.g. PRDXs and GPXs) had more decreased expression with time on ART in PWH with a less
447 pronounced effect in PrEP (**Fig. 4c**). Conversely, glutathione metabolism substrates used by GPXs to
448 neutralize free radicals, and glutathione reductase (*GSR*) had increased expression with time on ART in
449 PrEP (**Fig. 4c**). Overall, AM presented an unbalanced expression between effector enzymes and substrate
450 metabolism when coping with cellular stress. The UPR pathway plays a crucial role in maintaining
451 cellular homeostasis and encompasses three main branches via IRE1, PERK and ATF6. Notably, the
452 *ERN1* (IRE1), *EIF2AK3* (PERK) and *ATF6* genes had increased expression with time on ART in PWH
453 (**Fig. 4c**). The PERK branch genes also had increased expression with time on ART in PrEP (**Fig. 4c**).
454 Interestingly, at the epigenetic level, the promoters of *ERN1* and *EIF2AK3* were more active with
455 increased time on ART in both PrEP and PWH groups (**Fig. 4d**). Taken together, our data suggested a
456 dysregulated response to stress in AM with increased time on ART.
457 Accelerated cellular aging has been suggested as a candidate mechanism contributing to the
458 increased incidence of comorbidities in PWH. We found that the Cellular Senescence and Senescence
459 Associated Secretory Phenotype (SASP) gene sets correlated with time on ART (**Fig. 4b**). Senescence is a

460 complex mechanism that involves multiple cellular processes including DDR, cell cycle arrest, cellular
461 stress and cytokines mediating the immune response. Increased AP-1 activity, and levels of p21 (encoded
462 by *CDKN1A*), as well as Growth Arrest and DNA Damage-inducible genes (i.e. *GADD45A*) are
463 considered a hallmark of cellular senescence via cell cycle arrest (**Fig. 4c**). The *CDKN1A* promoter was
464 progressively more active with increased chromatin accessibility, H3K27ac and H3K4me3 marks, and
465 *CDKN1A* displayed increased expression with time on ART for both PrEP and PWH groups (**Fig. 4c and**
466 **4d**). Intriguingly, expression of *TP53* (p53) was decreased while *MDM2* (p53 inhibitor) expression was
467 increased with time on ART in PWH suggesting an imbalance of DDR in AM in PWH (**Fig. 4c**).
468 Moreover, key inducers of apoptosis such as *BBC3* (i.e. PUMA) and *BAX* had decreased expression with
469 time on ART while apoptosis inhibitors via caspase neutralization (e.g., *BCL2*, *XIAP*, and *BIRC2*) had
470 increased expression. Two independent terms captured the SASP state of AM including the SenMayo, a
471 well-established senescence gene set across tissues and species (**Fig. 4c**). In SASP high levels of
472 interleukins (IL-1 and IL-6 family), chemokines (CCLs and CXCLs), and MMPs are a sign of accelerated
473 cellular aging. Multiple SASP cytokine genes had increased expression with time on ART in AM from
474 both the PrEP and PWH group (**Fig. 4c**). The effect of time on ART on SASP key genes such as *CXCL8,*
475 *IL6R* and *IL36B* (IL-1 family member) were among the most significant changes at the transcriptomic and
476 epigenetic levels (**Fig. 4d; Table S4**). Taken together, our analysis of the effect of time on ART found
477 that AM of both groups displayed the epigenetic and transcriptomic characteristic of cells undergoing cell
478 cycle arrest senescence, reduced apoptosis with dysregulated DDR and a pro-inflammatory SASP profile.

479 When studying time on therapy as a variable there is potential for collinearity with chronological
480 age which may not be fully accounted for in statistical modeling. To address this, we evaluated the
481 correlation between time on ART and the chronological age of participants. No significant correlation
482 was detected between the participants' chronological age and time on ART in PrEP ($R = 0.001$, $p = 1$)
483 with a trend detected for PWH ($R = 0.40$, $p = 0.11$) (**Fig. S5a**). Next, we assessed if the chronological age
484 was a confounder in the association of senescence and TNF signaling pathways with time on ART in

485 PrEP and in PWH. We compared individual GESECA scores of these two pathways with chronological
486 age in AM from both groups and failed to detect any significant correlation (**Fig. S5b**). Another possible
487 confounder for the inflammatory and cell cycle arrest senescence-like status of AM is smoking. When
488 comparing individual GESECA scores for senescence and TNF signaling pathways we found no
489 association with smoking status (**Fig. S5c**). These observations reinforced the accuracy of our modeling in
490 accounting for confounders related to pathways associated with ART. Yet, this does not exclude the
491 independent contribution of ageing and smoking on the physiological state of AM, which was not
492 evaluated in the context of this study.

493 *Increased chromatin accessibility in AM with continuous exposure to ART is enriched for motifs and*
494 *footprints of pro-inflammatory and senescence associated TFs*

495 Given that the effect of time on ART was detected in both the PrEP and PWH groups for multiple
496 pathways, we tested the overall impact of continuous exposure to ART. We treated the HC group as a
497 time zero and assessed the effect of time on ART on AM physiology by combining all samples while
498 adjusting on the HC, PrEP and PWH status. We detected significant changes at FDR < 10% with
499 continuous exposure to ART in 26.7% of the regions with accessible chromatin, 22.4% of H3K27ac,
500 21.8% of H3K4me3, and 52.7% of expressed genes (**Fig. 5a; Table S3**).We then repeated the GESECA
501 analysis for the timepoints irrespective of the groups to recapitulate the correlation of biological pathways
502 with time on ART (**Fig. S6a**). For example, the TNF signaling pathway correlated with the continuous
503 exposure to ART, recapitulating the per group time effect (**Fig. S6b**). To showcase the effect of time on
504 ART at the epigenetic level, we derived chromatin traces representing promoter accessibility and active
505 histone marks for two AP-1 genes (*FOSL1*, *JUN*) and two AP-1 cooperators (*ATF3*, *ETS2*) (**Fig. 5b**).
506 These genes showed significantly increased expression with time on ART in AM from both PrEP and
507 PWH (**Fig. 4c)** and consequently in the combined analysis for continuous exposure to ART (**Table S3**).

508 The focus of the combined analysis was to evaluate the overall epigenetic regulation of ART on
509 the AM physiological state. Since expression of transcription factor (TF) genes, including AP-1 family

510 members, correlated with ART duration in AM from both PrEP and PWH, we tested if TF motifs and
511 footprints were enriched in chromatin regions showing differential accessibility with continuous ART
512 exposure.. First, we evaluated if chromatin accessibility changes with continuous exposure to ART were
513 enriched for motifs of TFs that supported a poised pro-inflammatory and senescent state of AM. We
514 estimated the frequency of TFs motifs cataloged by HOMER in two control groups: (i) 500,000 random
515 genomic regions (Random), and (ii) 20,060 ATAC regions with FDR > 50% (FDR50) for the continuous
516 exposure to ART. Next, we compared motif frequencies in the control groups with the 8177 increased and
517 8274 decreased differential chromatin sites with continuous exposure to ART (ATAC at **Fig. 5a and**
518 **Table S4**). We found 283 and 15 motifs significantly enriched (FDR < 1%) in regions with increased and
519 decreased accessibility with time on ART compared to the two control groups, respectively (**Table S4**).
520 Next, we performed TF binding clustering by motif similarities and identified 8 groups encompassing the
521 top 50 motifs with higher frequency in regions with increased accessibility with continuous exposure to
522 ART (**Fig. 5c**). Group 2 included motifs for the Early growth response (EGR) family; Group 3 motifs for
523 members of the KLF family; Group 5 motifs for MYC and MAFK; Group 6 motifs for AP-1 subunits
524 such as Fra1 (i.e *FOLS1*), FOSL2 and JUN, and AP-1 cooperative TFs such as ATF3 and BACH; and
525 Group 8 included members of the CRE and ATF family which crosstalk with multiple members of the
526 AP-1 complex (**Fig. 5d**). The majority of TFs included in the five largest groups displayed coordinated
527 effects where TFs with motifs enriched in chromatin regions with increased accessibility also showed
528 differential gene expression with time on ART (**Table S3; Fig. S7**). The enrichment of motifs in regions
529 with decreasing accessibility with time on ART was low. We found that 13 out of the 15 motifs with
530 higher frequency in regions with decreased chromatin accessibility versus FDR50 were part of a single
531 group including IRF and ELF genes (**Fig. 5d,** right).

532

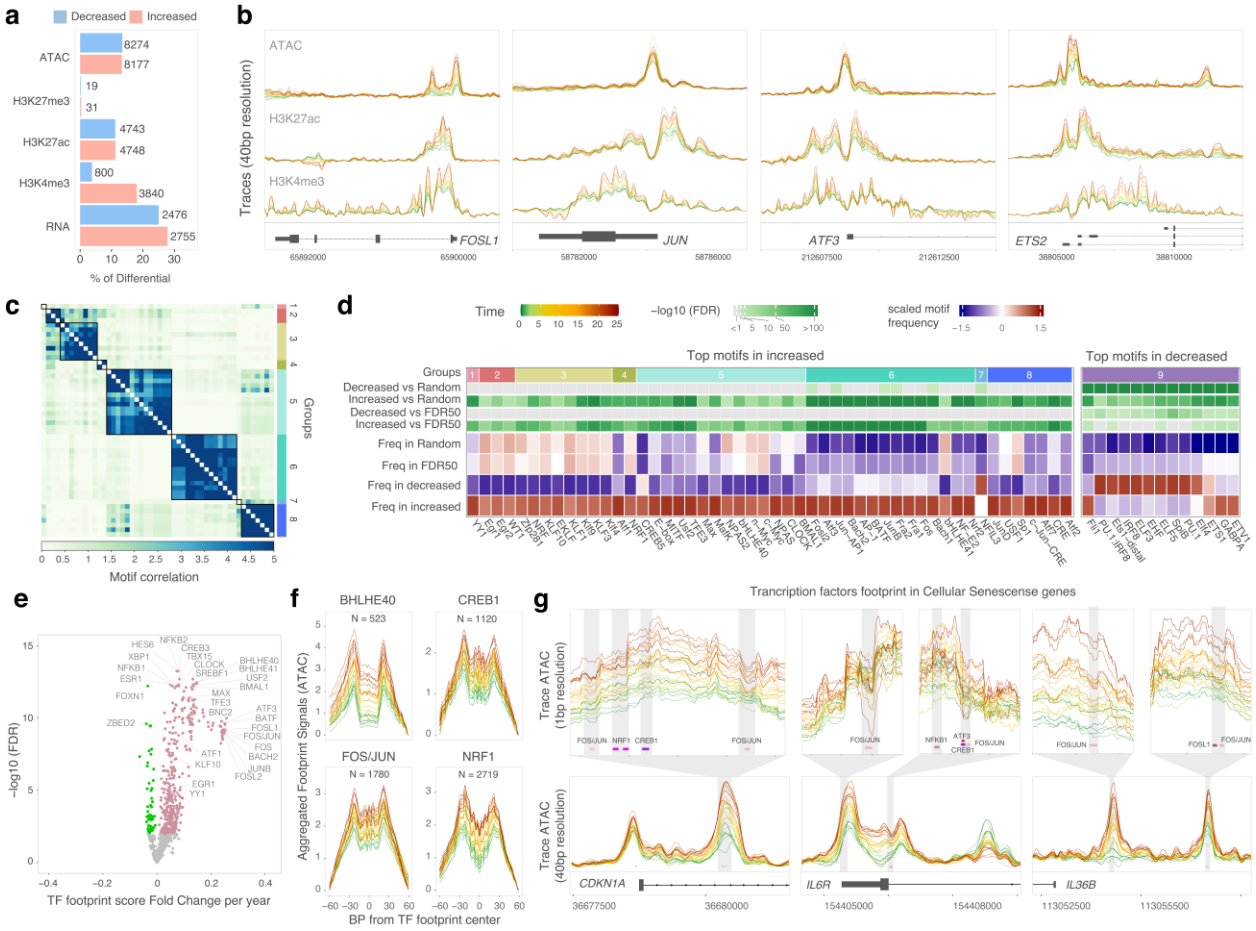

Fig. 5. The effect of continuous exposure to ART on the epigenetic regulation of AM physiology.

(**a**) Regions and genes affected by continuous exposure to ART. The bar plots show the proportion of affected regions/genes at an FDR < 10% relative to the total number of tested regions/genes. The absolute number of affected regions/genes are shown next to the bars. (**b**) Traces for chromatin accessibility, H3K27ac, and H3K4me3 marks at the promoter of four transcription factors (TF) of the TNF signaling pathway. Each line represents the normalized and covariate-corrected coverage for timepoints at a 40 base-pair (bp) resolution. (**c**) Hierarchical clustering the top 50 TF motifs found in regions with increased accessibility. (**d**) Motif frequency of the top TF motifs in the Decreased and Increased chromatin accessibility regions with continuous exposure to ART and the two control groups. The first row orders the motif-binding homology groups from "c". (**e**) TF footprint depth in regions with increased accessibility with continuous exposure to ART. (**f**) Examples of aggregated footprint signals for TFs

545 associated with continuous exposure to ART. Each line represents a timepoint of ART exposure. The
546 traces depict the average signal surrounding motifs for four significant TF. The signal was normalized for
547 the minimum signal per sample to start at 0. (**g**) Trace plots showing footprints of AP-1 subunits and
548 cooperators in the promoter of genes associated with senescence. A dampening in the ATAC trace signal
549 (i.e. valleys) indicates footprints on top of the motifs.
550
551 Next, we tested the differential TF occupancy (i.e. footprint) against continuous exposure to
552 ART. Of note, participants with the exact same time on ART were treated as a single timepoint. TF
553 footprints were detected via depletion of ATACseq signal overlapping TF motifs within higher flanking
554 ATACseq signals (i.e. valleys). A footprint score per timepoint was calculated for 919 JASPAR core
555 motifs over the 8177 regions with increased chromatin accessibility with continuous exposure to ART.
556 We then tested if the footprint mean score per TF (which is the average of footprint scores in all motifs
557 for a given TF) correlated with the continuous exposure to ART (**Table S5**). We identified a significant
558 increase in mean footprint score per year for 421 TFs and a significant decrease for 55 TFs (FDR < 1%)
559 (**Fig. 5e**). Among the TF footprints with the most pronounced fold change per year (FC > 0.2) were
560 members of the AP-1 family (**Fig. 5e**). Moreover, members of all motif groups that displayed higher
561 frequency in increased chromatin accessibility with time on ART had significantly stronger footprints
562 with time on ART (**Fig. 5d and 5e**). Compared to changes in TF footprint, the effect of continuous
563 exposure to ART was more apparent for chromatin accessibility (**Fig. 5f**). Yet, most striking was the
564 coordinated combined effect of accessibility and footprints and gene expression. For example, footprints
565 for AP-1 subunits and other TFs associated with time on ART were identified in the core promoter of
566 important genes mediating immune and senescence phenotypes. We detected footprints for the AP-1
567 JUN/FOS complex and other AP-1 cooperators in the TSS of *CDKN1A* (p21), *IL6R* and *IL36B* that are
568 key mediators of senescence (**Fig. 5g**). These footprints had a higher depth for footprint valleys in longer
569 ART regimens (**Fig. 5g**).
570

571 *Different proportions of distinct AM physiological states in PrEP and PWH*

572 We hypothesized that differences in the proportions of AM subpopulations of distinct
573 physiological state contribute to the epigenetic and transcriptomic group differences and the effects
574 associated with continuous exposure to ART. Given the time-independent effect of ART on interferon
575 signaling, we also hypothesized that ART impaired AM response to a virus challenge, as previously
576 observed for *Mtb* (17). To test these hypotheses, we used snMulti to identify differences in AM
577 subpopulation between HC, PrEP, and PWH, including their *ex vivo* response to SARS-CoV-2 challenge,
578 and the effects of continuous exposure to ART. We selected three participants per group, prioritizing
579 those with long-term ART in the PrEP and PWH groups (**Table 1**).

580 Quality control for the snMulti data was performed independently for the RNA and ATAC
581 modalities. Nuclei that passed QC in both modalities were used for multimodal integration to identify AM
582 clusters (**Fig. S8**). Seven distinct AM subpopulations, or "physiological states," named AM.0 to AM.6,
583 were identified (**Fig. 6a**). These subpopulations were independent of the SARS-CoV-2 challenge, as the
584 leading cluster markers were observed in both untreated and SARS-CoV-2–exposed AM (**Fig. 6b**). To
585 functionally annotate the state of each AM subpopulation, we performed gene ontology (GO) enrichment
586 analysis using cluster markers with FDR < 5% expressed in >25% of the AM subpopulation in
587 unchallenged samples to avoid potential bias from the SARS-CoV-2 challenge. The top GO term per
588 subpopulation defined the main physiological state of each AM cluster (**Fig. 6c**).

589 To assess AM state transitions and their modulation by group or SARS-CoV-2 challenge, we
590 performed trajectory and pseudotime analyses. In both approaches, the trajectories were not altered by
591 either phenotype group or SARS-CoV-2 challenge (**Fig. S9**). Next, we quantified the proportion of AM
592 subpopulations across phenotype groups (**Fig. 6d**). Participants on PrEP had a significantly lower
593 proportion of cells in the type-II interferon subpopulation AM.0 while PWH had a significantly lower
594 proportion in antigen presentation AM.4. Both PrEP and PWH showed a significantly higher proportion
595 of the AM.3 state which is characterized by endocytosis and is depleted of interferon responsive genes

596 (**Fig. 6d**). Only subpopulation AM.5 significantly increased in proportion following *ex vivo* SARS-CoV-2

597 challenge, independent of phenotype group (**Fig. 6e**)

598

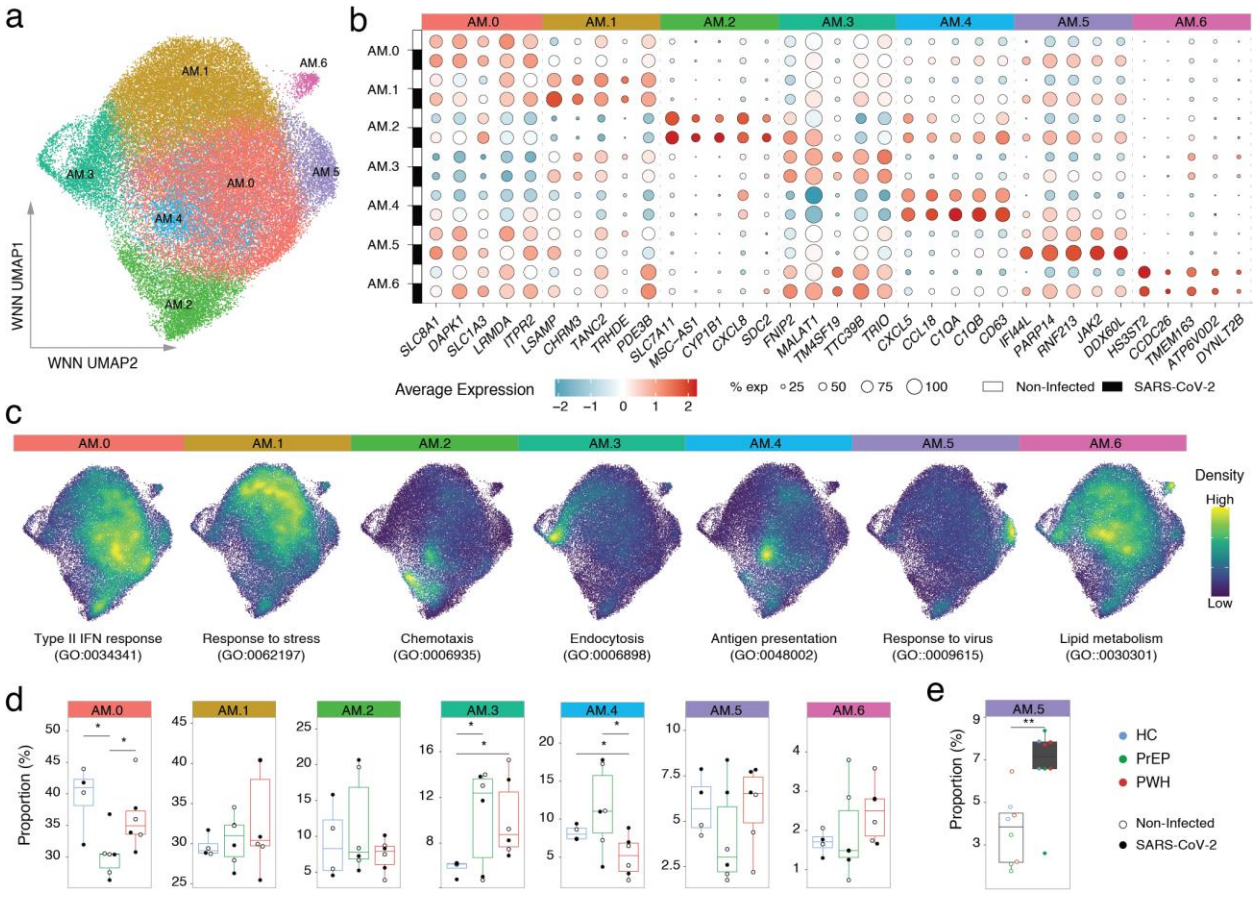

599

600 **Fig. 6. Participants on PrEP and PWH display different proportions of AM subpopulations**

601 **compared to healthy controls.**

602 (**a**) snMulti Uniform Manifold Approximation and Projection (UMAP) of 60,118 cells from HC, PrEP

603 and PWH participants either untreated or challenged with SARS-CoV-2. (**b**) Top 5 cluster markers for

604 each of the seven AM subpopulations split by SARS-CoV-2 challenge. (**c**) AM subpopulation

605 physiological state. A module score was calculated per cell using cluster markers assigned to the top GO

606 term of each AM subpopulation. The colours indicate the density of cells with high module scores for the

607 given gene ontology terms. (**d**) Proportion of AM subpopulations per group. Proportions are shown for

608 unchallenged, and SARS-CoV-2 challenged samples. (**e**) Increase in the AM5 cell proportion following
609 SARS-CoV-2 challenge. * *p*-value < 0.05, ** *p*-value < 0.01.
610
611 *Constitutive impaired interferon signaling in AM physiological states enriched in participants on ART*
612 We confirmed the main biological pathways associated with high inter-individual variability
613 observed in the bulk experiments in the snMulti (**Fig. 2b** and **Fig. 7a**). Using a pseudobulk approach per
614 AM subpopulation we observed that the most variable gene sets between participants included interferon
615 responses, MYC targets, OXPHOS, and TNF signaling via NFKB. This was consistent with the bulk-
616 level findings. The interferon gamma response gene set was equally significant across most AM
617 subpopulations while other gene sets were differently distributed across specific AM subsets (**Fig. 7a**).
618 Module scores per sample for the interferon gamma gene set indicate a global trend of reduced chromatin
619 accessibility and gene expression in participants on ART independent of infection (**Fig. 7b**). Notably,
620 participants on PrEP showed significantly lower module scores for chromatin accessibility in AM.3 and
621 AM.5, subpopulations representing the lowest and highest interferon response states, respectively (**Fig.
622 7b**). This constitutive impairment extended to core components of the interferon signaling pathway not
623 included in the hallmark gene set. For example, the single-nucleus expression of key mediators of type I,
624 II, and III interferon signaling has constitutively lower nuclear expression in AM from PrEP, and to a
625 lower extent from PWH, compared to HC (**Fig. 7c and Table S6**). This finding is in line with the time-
626 independent reduction of *IFNGR1* and *IFNAR2* expression detected in the cytoplasm of AM from PrEP at
627 the bulk stage (**Fig. 2e**). The transcriptional repression of interferon signaling was coordinated with
628 suppression of chromatin accessibility at the promoters of interferon receptors (e.g., *IFNGR1, IFNAR2,*
629 *IL10RB*) and downstream effectors (e.g., *STAT1*), across all subpopulations, including the polar extremes
630 AM.3 and AM.5 (**Fig. 7d**). The interferon gamma response gene set also included multiple antigen
631 presentation genes. We observed that participants on ART had reduced nuclear expression and promoter
632 accessibility of HLA genes (**Fig. S10 and Table S6**). This effect in HLA-DRA and the non-classical class

633 II molecules HLA-DM was consistent across both bulk and single nucleus profile (**Table S1** and **Table**
634 **S6**). Together, these results expand on the presence of a constitutively impaired interferon response state
635 in AMs of individuals on ART that was more pronounced in PrEP and in the AM.3 physiological state,
636 which is more frequent in AM isolated from PrEP and PWH participants. (**Fig. 6e**).

637 *Impaired AM response to SARS-CoV-2 ex vivo challenge in participants on ART*

638 Interferon signaling is a critical component of host defense against viral pathogens. Hence, we
639 tested if the constitutively reduced interferon signaling observed in AM in participants on ART affected
640 their ability to mount a robust epigenetic and transcriptomic response following *ex vivo* SARS-CoV-2
641 exposure. AM from HC showed significant transcriptional changes in response to the virus while both
642 PrEP and PWH showed few or no significant changes passing FDR < 10% (**Fig, 6e**, top and **Table S7**).
643 Across all AM subpopulations, the magnitude of nuclear transcriptional response to SARS-CoV-2 was
644 remarkably lower in participants on ART for the differentially expressed genes (**Fig, 6e**, bottom). As
645 expected, interferon related genes displayed the highest fold changes in response to SARS-CoV-2. The
646 most strongly induced genes were *IFI44L* and *RSAD2* (**Fig. 6e** and **6f**). In contrast, we detected only a
647 few significant chromatin accessibility changes following SARS-CoV-2 exposure, none of which were
648 enriched in a specific gene set. This lack of epigenetic response may reflect both the small sample size,
649 number of tests and the sparsity of snATAC data when analyzed at the pseudobulk level. Nevertheless,
650 we observed changes in chromatin accessibility at the promoters of interferon response genes, including
651 *IFI44L* and *RSAD2* (**Fig. 6g**). However, baseline differences in promoter accessibility between groups
652 were substantially more pronounced than the changes induced by SARS-CoV-2 (**Fig. 6g**).
653

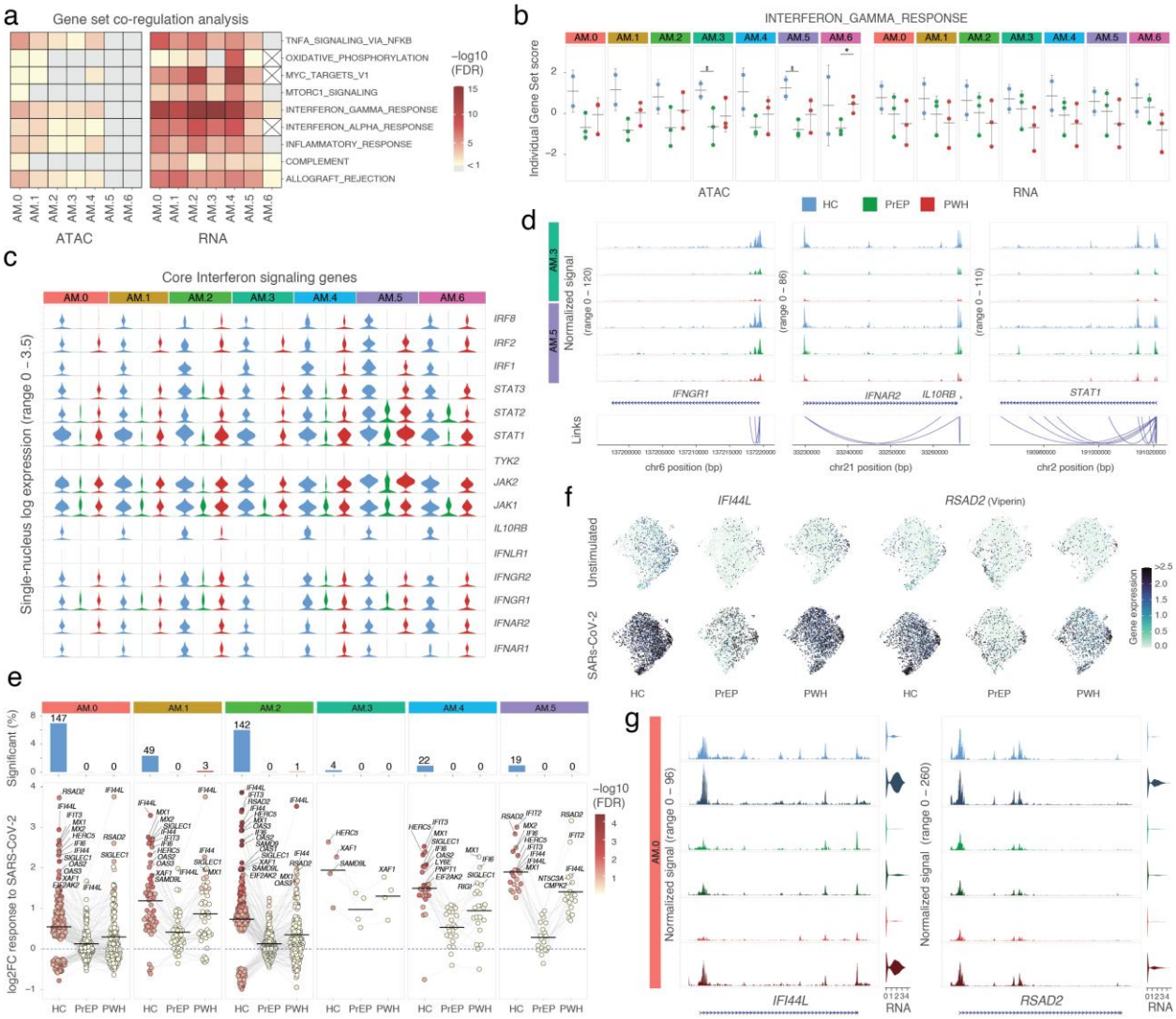

Fig. 6. Constitutive and SARS-CoV-2–induced interferon signaling is impaired in AM from participants on ART.

(**a**) GESECA hallmark gene sets with the largest variability between individuals. Gene sets with FDR < 10% in at least two assays for the same AM subpopulation are shown as a heatmap. **(b)** GESECA scores per subject and AM subpopulation separated by group for the interferon gamma response gene set. * t-test *p*-value < 0.05. (**c**) Single-nucleus expression of core interferon signaling genes. Violin plots indicate the per cell expression of the genes listed on the right. **(d)** Chromatin accessibility plots for three selected interferon response genes in the AM.3 and AM.5 subpopulations. Tracks display peaks representing baseline chromatin accessibility down sampled to show the same number of cells per group. The links

664 indicate the correlation of peaks and gene expression. **(e)** Differential transcriptomic response to SARS-
665 CoV-2 challenge. The top panel shows the proportion of differentially expressed genes at FDR < 10%
666 relative to the number of tested genes for each AM subpopulation with the absolute number indicated
667 above each bar. The bottom panel displays genes differentially expressed in at least one group for each
668 AM subpopulation plotted across all phenotype groups by their log2 fold change in response to SARS-
669 CoV-2. AM.6 was omitted due to absence of significant changes in any of the groups. The crossbar
670 indicates the median fold change, including both upregulated and downregulated genes. **(f)** snMulti
671 UMAP with gene expression of two genes of the interferon gamma gene set. **(g)** Chromatin accessibility
672 plots for the genes shown in panel f. Tracks were generated as in panel d and separated by group and
673 SARS-CoV-2 challenge status. Single-nucleus expression levels for each gene are shown on the right for
674 each condition.
675

676 *Single nucleus TF signature of senescence-like pro-inflammatory profile with continuous exposure to*
677 *ART*

678 We investigated if the senescence-like pro-inflammatory profile associated with continuous
679 exposure to ART was restricted to specific AM subpopulations. To address this, we performed
680 pseudobulk differential feature analysis for continuous exposure to ART stratified by AM subpopulation.
681 At the nuclear transcriptome level, subpopulations AM.0, AM.1 and, AM.2 had the highest proportions of
682 differentially expressed genes with continuous exposure to ART (**Fig. 7a**, top, and **Table S8**).
683 Interestingly, AM.3 displayed fewer differentially expressed genes compared to AM.4. Considering that
684 AM.3 encompass more cells than AM.4 it confirms the IFN attenuated physiological state of the
685 subpopulation enriched in PrEP and PWH in response to SARS-CoV2. Among the top differentially
686 expressed genes, the pro-inflammatory chemokine *CXCL5* showed the highest fold change per year on
687 ART, while the immunomodulatory *NRP2* showed the lowest (**Fig. 7b**). The expression of both genes
688 was accompanied by corresponding changes in promoter accessibility (**Fig. 7b**). In contrast, the count of

689 differentially accessible chromatin decreased accordingly to the number of cells per subpopulation (**Fig.**
690 **7a**, bottom, and **Table S8**). Several genes and chromatin regions associated with continuous exposure to
691 ART at the bulk stage were below detectability and could not be tested. Nevertheless, at the AM
692 subpopulation level, we observed the same trend of association with continuous exposure to ART for key
693 senescence markers, including *CXCL8* and the IL6 transducer *IL6ST* from SASP, as well as *MDM2*,
694 *BCL2,* and *E2F3,* which are involved in distinct mechanisms of senescence (**Fig. S11**).
695 We investigated the extent to which the senescence-like pro-inflammatory TF signature
696 associated with continuous exposure to ART at the bulk stage was captured by a specific AM
697 subpopulation. For that, we inferred TF activity based on the expression of known target genes either
698 induced or repressed by each TF. Using the differentially expressed genes identified per subpopulation
699 shown in Fig. 7a, we calculated TF activity scores per nucleus and tested their association with
700 continuous exposure to ART per AM subpopulation using a linear model. TF with absolute beta > 0.02
701 and FDR < 1% were considered significant (**Fig. 7c**). The results provided confirmation at the single
702 nucleus level of the bulk findings and indicate that the continuous exposure to ART effect is not restricted
703 to one AM subpopulation. We observed increased TF activity for AP-1 family members (e.g., JUN and
704 FOS) as well as other TFs identified through differential footprint analysis in the bulk stage (e.g.,
705 NFKB1, CREB1, ATF2, EGR1) with continuous exposure to ART (**Fig. 7c**). Conversely, interferon-
706 responsive factors (IRFs) showed decreased activity, consistent with the reduced motif enrichment
707 observed with continuous exposure to ART in the bulk stage (**Fig. 4d** and **Fig. 7c**). The senescence-like
708 TF signature was more pronounced in subpopulations AM.0, AM.1, and AM.4. However, this may be a
709 reflection of the higher number of differentially expressed genes which are used to assess TF activity.
710 The TF activity analysis considered only the snRNA modality. To harness the full power of
711 snMulti we performed a TF gene regulatory network (GRN) analysis using the differential features from
712 the ATAC and RNA modalities shown in Fig. 7a. For each TF we modeled gene expression as a function
713 of the interaction between chromatin accessibility at regions containing the TF motif and the TF's
714 expression across single nuclei using Pando framework. TF–target gene connections with FDR < 10%

715 were considered significant. We performed the analysis for all AM subpopulations combined. TFs with
716 more than 50 significant connections included the core regulator of pro-inflammatory signaling (NFKB1)
717 and senescence-associated TFs (e.g., JUN, ETS2 and KLF6) (**Fig. 7d)**. Next, we estimated a global GRN
718 module comprising co-regulated TF–target gene signatures (**Fig. 7e**). This network reflects the
719 coordinated effect of key TFs in regulating differential gene expression. A central TF in the global GRN
720 was NFKB1, which, together with HIF1A, ETS2, and KLF6, underlines the senescence-like pro-
721 inflammatory state of AM at the single-nucleus level (**Fig. 7f**). Establishment of the TF hierarchy allows
722 the targeting of key TF for improved or adjuvant therapy.
723 A limitation of the snMulti GRN approach is that it strongly relies on TF expression modeling,
724 which can be challenging in highly differentiated cells like AM with low baseline TF expression, and
725 number of nuclei. As a result, GRN analysis stratified by subpopulation was feasible only for larger
726 subpopulations such as AM.0 with sufficient number of nuclei. Nevertheless, in AM.0 we captured part of
727 the GRN modules identified in the combined AM subpopulations. Importantly, the senescence-like pro-
728 inflammatory signature driven by NFKB1, ETS2, and KLF6 was still observed, likely because it was not
729 specific but rather shared across multiple AM subpopulations. This suggested that the senescence-like
730 pro-inflammatory profile was not restricted to a single AM subpopulation and was consistent with both
731 the bulk-level observations and the TF activity inferred from snRNA. Taken together, these results
732 reinforced the presence of a TF signature consistent with a senescence-like pro-inflammatory profile in
733 AMs of participants with continuous exposure to ART.
734

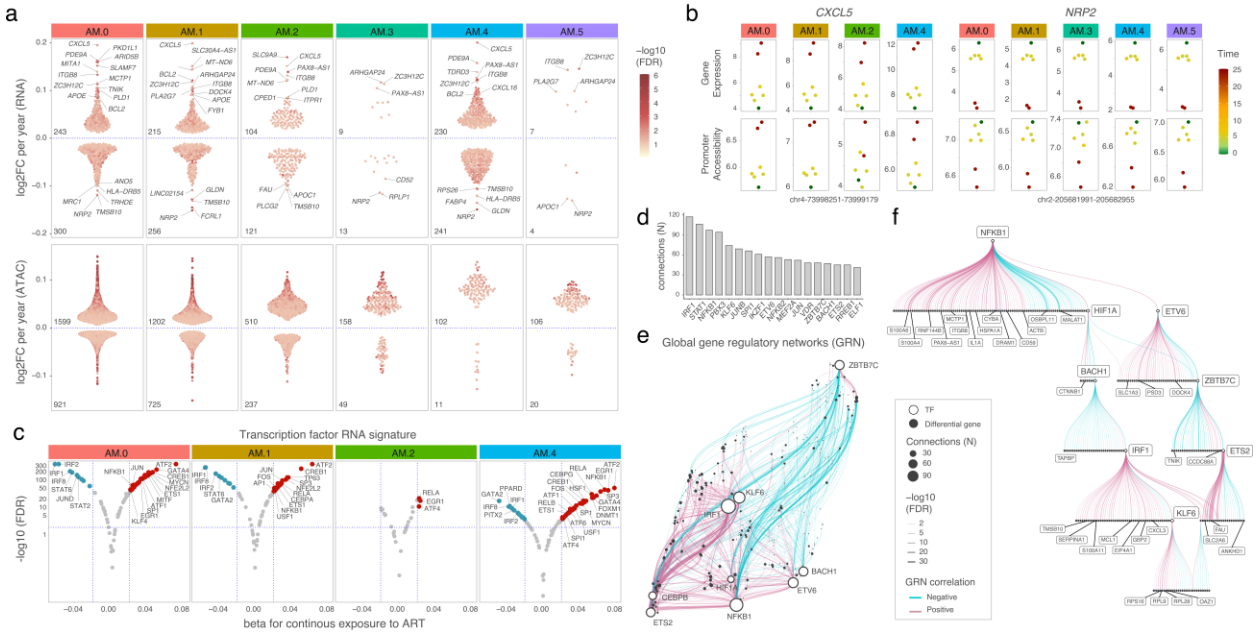

Fig. 7. Coordinated TF activity indicates a senescence-like pro-inflammatory profile in AMs with continuous exposure to ART.

(**a**) Differential features associated with continuous exposure to ART for snRNA and snATAC. Differential features with FDR < 10% were plotted according to the log2 fold change per year of ART exposure per AM subpopulations. (**b**) Top genes differentially up- (*CXCL5*) or down-regulated (*NRP2*) with continuous exposure to ART. (**c**) TF activity scores with continuous exposure to ART. The x-axis shows beta coefficients for the association between single-nucleus TF activity and continuous exposure to ART. The y-axis shows the corresponding FDR *p*-values. Red and blue indicating increased and decreased activity, respectively. **(d–f)** snMulti Gene Regulatory Network (GRN) analysis based on the 3,332 unique differential chromatin regions and 867 differential genes identified in panel "a". (**d**) The y-axis indicates the number of differential genes (N) connected to differential regions containing motifs for the corresponding TFs shown on the x-axis. Only TFs with more than 50 significant connections are displayed. (**e**) Global GRN module. The network shows connections between TFs and their associated target genes. Edge color indicates the direction of the correlation and edge width the statistical FDR of the connection. (**f**) TF subnetwork highlighting NFKB1 position at the top of a cascade within the GRN. Each circle in the hierarchical tree represents a target gene of the TF network.

752 **Discussion**

753 We found two major effects of NRTI-based ART in AM. First, interferon responses were
754 impaired both at basal and following a viral challenge with stronger effect in HIV-negative PrEP
755 participants and independent of ART duration. Second, continuous ART exposure reshaped AM
756 homeostasis and cellular state at the epigenetic and transcriptomic levels. Both PWH and PrEP
757 participants showed a progressive senescence-like pro-inflammatory profile that correlated with duration
758 of NRTI exposure.

759 Cellular senescence encompasses multiple biological processes and is often referred to as the
760 "zombie cell" state, in which cells are under growth-arrest and resistant to apoptosis while remaining
761 metabolically and transcriptionally active. These cells are viable despite their cytotoxic microenvironment
762 but display an impaired ability to execute their proper physiological role. In our study, AM from both
763 PrEP and PWH participants exhibited epigenetic and transcriptomic features consistent with this state.
764 Genes involved in cycle arrest, such as *CDKN1A* (p21), *CHEK2*, and *GADD45A* had increased expression
765 with longer ART duration, while *GADD45B* expression was elevated in both PrEP and PWH AM,
766 independent of time on ART. These proteins mediate G2 phase arrest, preventing progression to the M
767 phase (52-54). Concurrently, key pro-apoptotic inducers such as *BAX* and *BBC3* (PUMA) were
768 downregulated, while anti-apoptotic genes such as *BCL2*, *XIAP* and *BIRC2* were upregulated with
769 increased time on ART. Together, these gene expression changes suggest that viable AM are at least
770 partially trapped in the G2 phase which combined with the cellular and mitochondrial stress and pro-
771 inflammatory SASP profile could be detrimental to their cellular function. Another aspect is paracrine
772 senescence in which SASP cytokines propagate the senescent state to neighboring cells (55). In this
773 context, the effects of continuous NRTI-based ART are likely not exclusive to AM but rather systemic.
774 Supporting this, studies in PWH on long-term ART have shown elevated plasma levels of SASP
775 cytokines such as IL-8, TNF, MMP-1, and CCLs which is consistent with our transcriptomic findings in
776 AM (56, 57). Additionally, NRTI exposure in astrocytes has been shown to induce p21, secretion of IL-1
777 family members, and activation of NF-κB p65, accompanied by increased ROS production and

778 mitochondrial dysfunction (58). Such systemic ART effects may be undetectable during short-term ART
779 or masked by the intertwined relationship with HIV infection. However, in analogy to the time
780 dependency of transcriptomic changes they might accumulate over the years potentially affecting cellular
781 function in multiple tissues. Such a detrimental effect on AM function has been shown directly through
782 the abrogated AM responses to both SARS-CoV2 and *Mycobacterium tuberculosis* (17).

783 Aging PWH on ART have a higher incidence of chronic airway diseases, including COPD, lung
784 fibrosis, and asthma, as well as a higher burden and early onset of lung cancers compared to ART-naive
785 individuals (59, 60). AM genes displaying differential expression with time on ART in our study have
786 been implicated in the pathogenesis of these conditions. For example, increased expression of AP-1
787 subunits in macrophages promotes tissue remodeling in COPD and lung fibrosis (61, 62). Moreover,
788 SASP cytokines such as IL-6 and IL-8 were observed to be elevated in the serum and BAL fluid of
789 patients with COPD and asthma (63-65). SASP is also characterized by increased oxidative stress and
790 overproduction of ROS by mitochondria or reduced antioxidant capacity (59, 66). In our study, we
791 detected an impaired expression of major antioxidant enzymes with longer time on ART. Oxidative
792 stress-based therapeutics are under investigation as candidates to treat the underlying pathogenic
793 mechanisms of COPD (67). Although AM are not a typically metastatic cells, they shape the tumor
794 microenvironment in the lung (68). Increased expression of AP-1 subunits *FOSL1* and *JUN* regulated
795 acquired resistance to treatment in non-small cell lung carcinoma (NSCLC), which was reversed with AP-
796 1 inhibitors (69). Another key oncogenic pathway is the p53-MDM2 loop. We observed *TP53*
797 downregulated with increased time on ART in PWH with a corresponding increased expression of its
798 antagonist *MDM2* in both PWH and PrEP participants. *MDM2* overexpression is a common feature in
799 lung cancers and the MDM2-p53 loop contributes to chemotherapeutic resistance in human malignancies
800 (70, 71). More broadly, we detected impairment of DDR mechanisms and cell cycle checkpoints in AM
801 from both PWH and PrEP, suggesting that prolonged ART may in part explain the increased
802 susceptibility to lung cancer in PWH.

803 Tuberculosis, pneumonia and more recently COVID-19 are major causes of death in PWH under
804 ART (14-16, 72). We previously showed that AM obtained from PWH and people on PrEP had a
805 diminished transcriptomic and epigenetic response to *Mtb* and here we extended these findings to SARS-
806 CoV-2 (17, 73-75). Interferons are key modulators of pulmonary host defense and the overall decreased
807 IFN mediated response we observed impaired the capacity of AM to mount a robust response to these two
808 distinct pulmonary pathogens (76). IFN neutralizing autoantibodies have been shown more frequently in
809 people with severe COVID-19 and in life-threatening COVID-19 pneumonia, which strengthens the
810 importance of a balanced interferon responses in the outcome of SARS-CoV-2 infection (77, 78). Of
811 relevance is the lower IFN receptors expression in AM from PrEP participants independent of time on
812 ART which was accompanied by an increased proportion of unresponsive AM subpopulations. While we
813 do not know if the blunted AM response to *ex vivo* SARS-CoV-2 challenge does have a major impact on
814 COVID-19 outcomes in people on PrEP, our results support the need for more detailed longitudinal
815 epidemiological data to assess the clinical implications of our findings. However, assuming that an
816 increased and wider scale of PrEP uptake may involve medicating millions of healthy people with NRTI,
817 potential side effects need to be further pondered either through the use of alternative ART classes or with
818 adjuvant therapies particularly in low HIV endemic settings (79).
819 PrEP is a highly effective strategy to prevent HIV acquisition (80). Our study does not advocate
820 against PrEP rollout in any way as protection from HIV infection dramatically outweighs potential ART
821 side effects. PrEP rollout in high exposure settings contributes to the decline of HIV diagnosis at the
822 population level and discontinuation, intermittent use or low PrEP compliance are known to reduce
823 prevention effectiveness (81-85). A few studies have highlighted adverse effects by short term exposure
824 to the most common NRTIs tenofovir disoproxil fumarate (TDF) and emtricitabine (FTC). Short term
825 TDF/FTC exposure induced tissue-specific IFN transcriptional signatures with upregulation of IFN-
826 response in the gut and downregulation in PBMCs and blood (86). Leukocytes exposed to TDF/FTC
827 displayed increased ROS production and lipid uptake and decreased mitochondrial mass and efferocytosis
828 (87, 88). NRTI exposure in monocyte-derived macrophages caused mitochondrial dysfunction, higher

829 levels of ROS and induction of SASP cytokines IL-6, IL-1β and TNF (89). Moreover, TDF was shown to
830 inhibit *in vitro* telomerase activity in PBMC from PWH (90). Combined these observations on short term
831 exposure to ART suggests a senescence-like profile in immune cells induced by NRTI. However, the
832 mechanisms by which long-term NRTI-based ART impacts cell physiology independent of HIV remains
833 largely unknown.

834 A strength of the snMulti is the ability to evaluate regulatory networks linking chromatin
835 accessibility and transcription factors with their target genes at each individual nucleus. We applied this
836 powerful approach to investigate the gene regulatory network that underlie the adverse effects of long-
837 term ART. We identified key transcriptions factors in central regulatory hubs modulating the
838 transcriptional changes associated with ART. However, targeting these key transcription factors is
839 challenging as many hubs lack pharmacological modulators or are considered undruggable due to their
840 essential and widespread functions such as the central hub of NFKB. However, engineered exosome
841 delivery technologies are being developed to specifically modulate NFKB activity by delivering long-
842 lasting super-repressor inhibitor of NFKB (Exo-srIκB). The Exo-srIκB system has been tested in rodent
843 models of kidney ischemia (91), sepsis (92)and age-related neuroinflammation (93). While these animal
844 studies are promising the exosome system currently lacks cell specificity. Moreover, in the context of
845 ART systemic inhibition of NFKB may itself could cause adverse effects that outweigh potential benefits.
846 By contrast, a possible exception among the key hubs we identified is HIF1A, for which a range of
847 pharmacological modulators have been developed and evaluated in pre-clinical and clinical studies (94).
848 Currently, the main clinical trials focus on ischemic disease and specific cancers rather than pathways of
849 immune activation (95, 96). Nevertheless, targeting of HIF1A may represent an alternative or
850 complementary approach to targeting senescence beyond senolytics in person on long term ART. While
851 HIF1A as modifiable target is attractive, the fact that adverse ART effects in AM require prolonged
852 exposure means that clinical trials would face extensive logistical challenges. This further supports the
853 rationale to study ART-adverse effect in cells other than AM. In such cells adverse effects may emerge
854 more rapidly and might provide useful biomarkers for interventional studies.

855 Our study has some limitations. AM are not an optimal cell type to evaluate the systemic effects
856 of NRTI-based ART. Our rationale for focusing on AM was based on our previous observation of a
857 blunted transcriptomic and epigenetic response to *Mtb* in both PrEP and PWH. The extent to which this
858 localized effect in the lung reflects systemic immune alterations remains unknown. Future systems-level
859 studies assessing circulating or progenitor cells combined with immediate clinically relevant assays (e.g.,
860 protein production) will be required to evaluate the long-term effects of ART on clinical outcomes.
861 Moreover, of the participant in the PrEP and PWH groups only one was female. Therefore, with our
862 dataset it is not possible to test a sex bias of the ART effect. Sex is associated with different levels of drug
863 metabolism, which might impact the ART effect in females. Participants of the PrEP group were more
864 homogeneous using the same NRTI ART regimen while in the PWH group, participants had more
865 complex therapies. PWH were exposed to multiple and different types of ART drugs throughout their life.
866 Exposure to older and more toxic ART might have contributed to the DNA damage observed in AM from
867 PWH. Importantly, our study did not allow to address the mechanisms and the ART drug concentration
868 that underlie the *in vivo* senescence-like pro-inflammatory state of AM.
869 Our study has several unique strengths. First, it is the only study to date that evaluated the long-
870 term epigenetic effect of ART in the HIV^+ and HIV^- context. Second, studies of PrEP side effects in
871 healthy subjects have relative short follow-up periods ranging from a few months to about a year. In
872 contrast, our retrospective cross-sectional approach evaluated a much longer effect of ART which would
873 be challenging to implement in a longitudinal design. Additionally, participants of the PrEP and PWH
874 groups did not include opioid users, and both groups have similar numbers of cannabis users.. Another
875 aspect is that studies on ART focused on PWH, making it difficult to separate the HIV-effect from the
876 ART-effect. Our study addressed this gap by studying ART effects in both HIV^+ and HIV^- persons
877 allowing us to identify specific ART-effects. Our study included three PHW with aprox. 10 years gap
878 between HIV diagnosis an ART initiation. These participants showed an AM profile that was in line with
879 the time on ART and not with the time from HIV diagnosis, which reinforced the role of NRTI-based
880 ART in the AM physiological state.

881 Most importantly, our study highlights the constant need for improved drug designs and
882 multidrug therapies to mitigate side effects. Treatment and prevention of HIV infection have come a long
883 way since the introduction of the first generation of highly toxic ART (e.g., zidovudine, stavudine,
884 didanosine). However, our study indicates the gaps that still need to be addressed towards improved
885 treatment to ensure the best quality of life for ART users. If the discovered effect is exclusive to the NRTI
886 class adjuvant therapies could be beneficial. For example, senolytics have been shown to mitigate cellular
887 senescence with compounds such as dasatinib, quercetin, and fisetin currently being tested in clinical
888 trials for pulmonary diseases linked to senescence (97, 98). Alternatively, drugs with distinct mechanisms
889 of action could potentially circumvent the side effects of long-term NRTI-based ART. Long-lasting
890 injectables, such as the HIV integrase inhibitor Cabotegravir and the capsid inhibitor lenacapavir, have
891 been investigated or approved as potential PrEP regimens (99-102). Albeit for most people at risk of HIV
892 acquisition the efficacy of PrEP outweighs the risks of potential side effects; our results suggest that
893 lengthy and continuous exposure to ART requires a highly judicious use, particularly for diseases where
894 AM play a critical role.

895 **Declarations**

896 *Ethics approval and consent to participate*

897 The study was approved by the Research Ethics Board of the McGill University Health Center (MUHC)
898 (MP-CUSM-15-406). All participants signed a written informed consent and were recruited at the McGill
899 University Health Centre (MUHC, Montreal, Canada).

900

901 *Consent for publication*

902 Not applicable

903

904 *Availability of data and materials*

905 The raw sequencing and processed datasets for the bulk and snMulti assays were deposited to GEO with
906 accession numbers XXXX. Additional data are available from the corresponding author on reasonable
907 request.

908

909 *Competing interests*

910 The authors declare that they have no competing interests

911

912 *Funding*

913 This work was supported by grant 487046 from the Canadian Institutes of Health Research (CIHR) to ES.
914 This research was supported through a resource allocation in the Cedar high performance computing
915 cluster by Compute Canada and WestGrid.

916 *Acknowledgements*

917 We thank all volunteers who participated in this study. We thank the members of bronchoscopy team at
918 MUHC, the members of the Routy and Costiniuk labs, and all members of the Schurr lab for their help
919 and discussions.

920

Table 1. Characteristics of enrolled subjects.

Sample	Group	Sex	Age	Smoker [a]	ART regiment	Molecules	Duration of HIV	Time on ART [b]	RNA	ATAC	H3K27ac	H3K27me3	H3K4me3	snMulti
AMC2	HC	M	56 – 60	YES	.	.	.	0	X	X	.	.	.	.
AMC7	HC	M	46 – 50	NO	.	.	.	0	X	X	.	.	.	.
AMC8	HC	M	21 – 25	NO	.	.	.	0	X	.	.	.	.	.
AMC9	HC	M	56 – 60	YES	.	.	.	0	X	X	X	X	X	.
AMC10	HC	M	26 – 30	NO	.	.	.	0	X	X	X	.	X	.
AMC11	HC	M	26 – 30	NO	.	.	.	0	X	X	X	.	.	.
AMC12	HC	M	35 – 40	NO	.	.	.	0	X	X	X	.	X	.
AMC12.2 [c]	HC	M	41 – 45	NO	.	.	.	0	.	.	.	.	.	X
AMC13	HC	F	35 – 40	NO	.	.	.	0	X	X	X	X	X	.
AMC14	HC	F	35 – 40	YES	.	.	.	0	X	X	.	X	.	.
AMC15	HC	F	41 – 45	NO	.	.	.	0	X	X	.	.	.	.
AMC16	HC	F	35 – 40	NO	.	.	.	0	X	X	.	.	.	.
AMC18	HC	M	26 – 30	NO	.	.	.	0	X	X	.	.	.	.
AMC19	HC	M	51 – 55	NO	.	.	.	0	X	X	.	.	.	.
AMC22	HC	F	41 – 45	YES	.	.	.	0	X	X	X	X	X	.
AMC38	HC	M	51 – 55	NO	.	.	.	0	.	.	.	.	.	X
AMP33	PrEP	M	26 – 30	NO	Truvada	Emtricitabine, Tenofovir	.	0.1	X	X	X	.	X	.
AMP35	PrEP	M	21 – 25	YES	Truvada	Emtricitabine, Tenofovir	.	1.0	X	X	X	X	X	.
AMP32	PrEP	M	35 – 40	NO	Truvada	Emtricitabine, Tenofovir	.	1.1	X	X	.	.	.	
AMP23	PrEP	M	61 – 65	YES	Truvada	Emtricitabine, Tenofovir	.	1.3	X	.	.	.	.	.
AMP30	PrEP	M	26 – 30	NO	Truvada	Emtricitabine, Tenofovir	.	2.4	X	.	.	.	.	.
AMP31	PrEP	M	35 – 40	NO	Truvada	Emtricitabine, Tenofovir	.	2.5	X	X	.	.	.	.
AMP34	PrEP	M	41 – 45	NO	Truvada	Emtricitabine, Tenofovir	.	3.2	X	X	X	.	.	.
AMP36	PrEP	M	26 – 30	YES	Truvada	Emtricitabine, Tenofovir	.	3.4	X	X	X	X	X	.
AMP27	PrEP	M	35 – 40	NO	Truvada	Emtricitabine, Tenofovir	.	4.4	X	X	X	X	X	.
AMP32.2 [c]	PrEP	M	35 – 40	NO	Truvada	Emtricitabine, Tenofovir	.	4.3	.	.	X	X	X	.
AMP32.3 [c]	PrEP	M	41 – 45	NO	Truvada	Emtricitabine, Tenofovir	.	5.2	.	.	.	.	.	X

AMP29	PrEP	M	35 – 40	YES	Truvada	Emtricitabine, Tenofovir	.	5.4	.	X	.	.	.	.
AMP23.2 [c]	PrEP	M	66 – 70	YES	Truvada	Emtricitabine, Tenofovir	.	5.9	.	.	.	.	.	X
AMP36.2 [c]	PrEP	M	31 – 35	YES	Truvada	Emtricitabine, Tenofovir	.	6.5	.	.	.	.	.	X
AMV23	PWH	M	31 – 35	YES	Genvoya	Emtricitabine, Tenofovir, Cobicistat, Elvitegravir	0.7	0.6	X	X	X	X	X	.
AMV27	PWH	M	56 – 60	NO	Descovy, Isentress	Emtricitabine, Tenofovir, Raltegravir	1.1	1.0	X	X	.	.	.	.
AMV17	PWH	M	41 – 45	YES	Viread, Tivicay, Edurant	Tenofovir, Dolutegravir, Rilpivirine	3.7	2.7	X	X	X	X	X	.
AMV23.2 [c]	PWH	M	35 – 40	YES	Genvoya	Emtricitabine, Tenofovir, Cobicistat, Elvitegravir			.	.	.	.	.	X
AMV21	PWH	M	61 – 65	YES	Truvada, Tivicay	Emtricitabine, Tenofovir, Dolutegravir	6.2	5.7	X	X	X	X	X	.
AMV5	PWH	M	56 – 60	NO	Truvada	Emtricitabine, Tenofovir	21.5	8.5	X	X	.	.	.	.
AMV26	PWH	M	46 – 50	NO	Atripla	Emtricitabine, Tenofovir, Efavirenz	18.4	8.5	X	X	.	.	.	.
AMV25	PWH	M	56 – 60	NO	Atripla	Emtricitabine, Tenofovir, Efavirenz	11.6	11.3	.	X	X	.	X	.
AMV19	PWH	M	56 – 60	YES	Triumeq	Abacavir, Dolutegravir, Lamivudine	12.7	11.4	X	X	.	.	.	.
AMV15	PWH	M	51 – 55	NO	Triumeq	Abacavir, Dolutegravir, Lamivudine	14.1	13.7	X	X	X	X	X	.
AMV9	PWH	M	56 – 60	YES	Truvada, Isentress	Emtricitabine, Tenofovir, Raltegravir	14.8	13.8	X	X	X	.	.	.
AMV16	PWH	M	56 – 60	YES	Genvoya	Emtricitabine, Tenofovir, Cobicistat, Elvitegravir	30.1	15.7	X	.	X	X	X	.
AMV4	PWH	M	56 – 60	YES	Biktarvy	Emtricitabine, Tenofovir, Bictegravir	17.0	17.0	X	X	X	.	.	.
AMV11	PWH	M	46 – 50	YES	Complera	Emtricitabine, Tenofovir, Rilpivirine	19.9	18.9	X	X	X	X	X	.
AMV3	PWH	M	51 – 55	NO	Truvada, Isentress	Emtricitabine, Tenofovir, Raltegravir	21.4	19.4	X	X	.	.	.	.
AMV14	PWH	M	56 – 60	YES	Kivexa, Reyataz, Norvir	Abacavir, Lamivudine, Atazanavir, Ritonavir	21.2	20.5	X	X	X	X	.	.
AMV20	PWH	M	56 – 60	YES	Truvada, Tybost, Prezista	Emtricitabine, Tenofovir, Cobiscistat, Darunavir	21.3	20.7	X	X	.	.	.	.
AMV10	PWH	M	56 – 60	NO	Intelence, Prezista, Tivicay, Norvir	Etravirine, Darunavir, Dolutegravir, Ritonavir	25.4	21.5	X	X	.	.	.	.
AMV13	PWH	F	51 – 55	YES	Complera, Reyataz, Isentress	Emtricitabine, Tenofovir, Rilpivirine, Atazanavir, Raltegravir	23.1	23.1	X	X	X	X	X	.
AMV11.2 [c]	PWH	M	56 – 60	YES	Complera	Emtricitabine, Tenofovir, Rilpivirine	25.8	24.2	.	.	.	.	.	X
AMV3.2 [c]	PWH	M	56 – 60	NO	Truvada, Isentress	Emtricitabine, Tenofovir, Raltegravir	27.1	25.1	.	.	.	.	.	X

[a] Cigarettes and/or cannabis. [b] Fraction of years from the ART start to BAL collection. [c] BALs of the same subject collected at different dates. ART, antiretroviral therapy; BAL, bronchoalveolar lavage, HC, healthy controls; PrEP healthy subject on pre-exposure prophylaxis; PWH, people with HIV under ART; an X indicate samples employed in each of the five tested assays.

Supplementary Materials

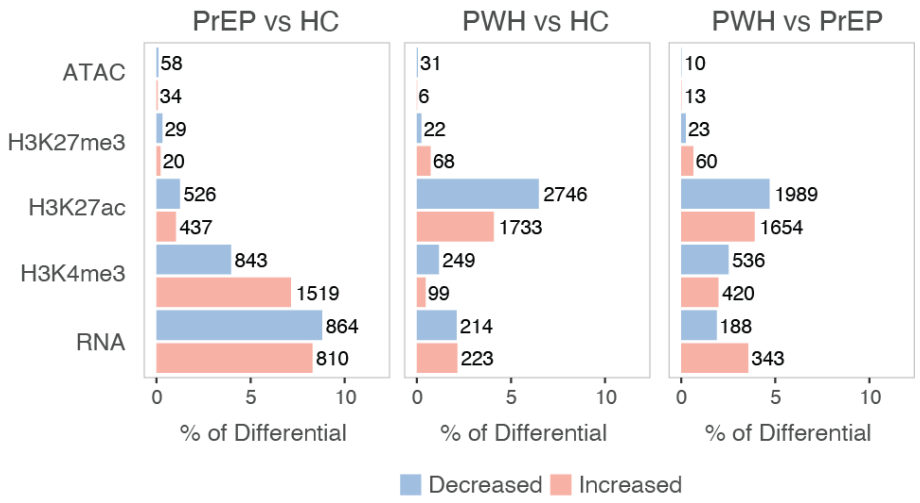

Fig. S1. Differential epigenetic and transcriptomic features between groups.

Differential epigenetic and transcriptomic features between groups are shown for the three baseline comparisons. The bar plots show the proportion of differential regions/genes at an FDR of 10% and absolute log2FC > 0.2 relative to the total number of tested regions/genes for time on ART in PrEP vs HC (left), PWH vs HC (center) and PWH vs PrEP (right). The absolute number of differential regions/genes are shown next to the bars. Decreased and increased DNA accessibility, histone marks, and gene expression are shown in blue and red, respectively.

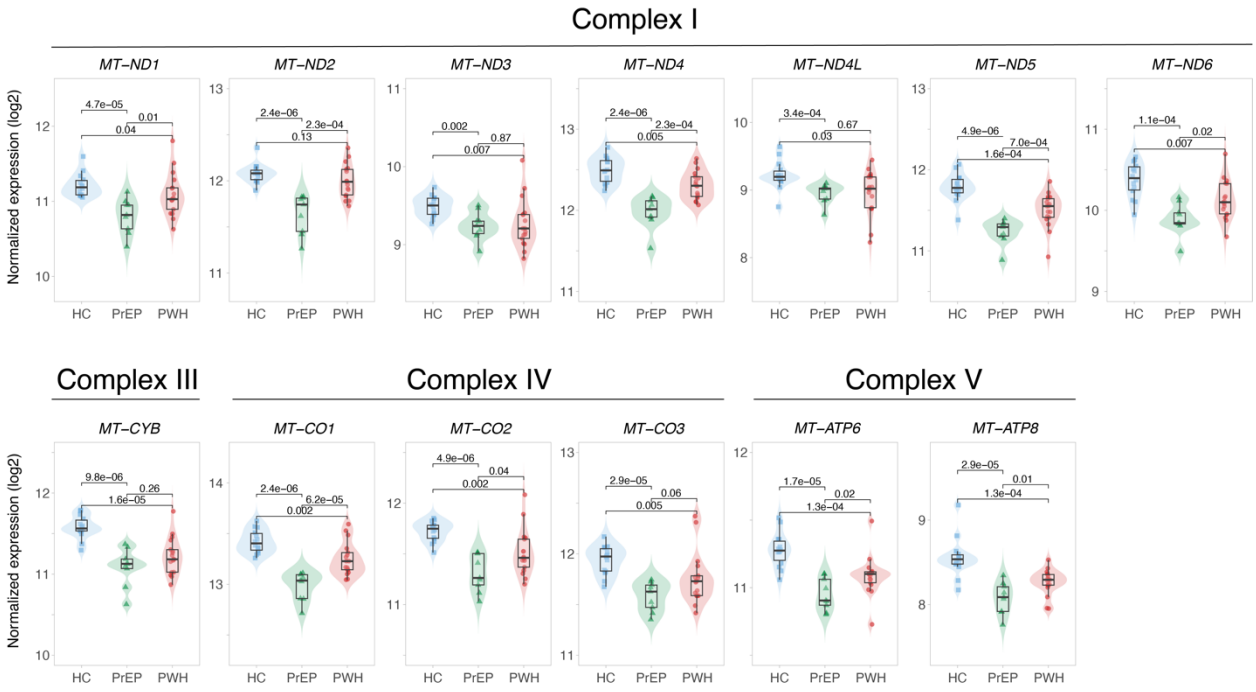

Fig. S2. Reduced expression of mitochondrial genes encoding enzymes of the electron transport chain.

Normalized gene expression per subject and group for mitochondrial genes encoding proteins of the human electron transport chain. *p*-values for the Wilcoxon test comparing differences in median expressions between groups are shown at the top.

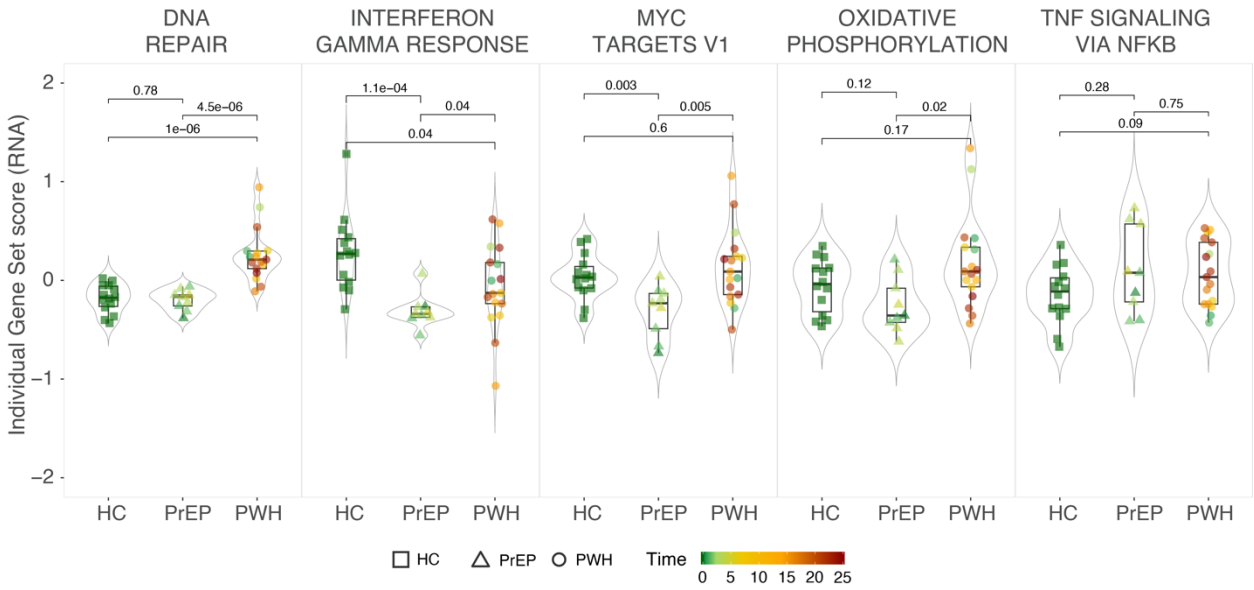

Fig. S3. Comparison between GESECA scores and phenotypic groups as in Fig. 2C indicating time on ART.

GESECA scores for the transcriptomic assay for each subject are plotted on the y-axis separated by phenotypic group on the x-axis. The *p*-values shown at the top are for the group compassions shown in Fig. 2C. The colour shades indicate the length of time on ART for PrEP and for PWH.

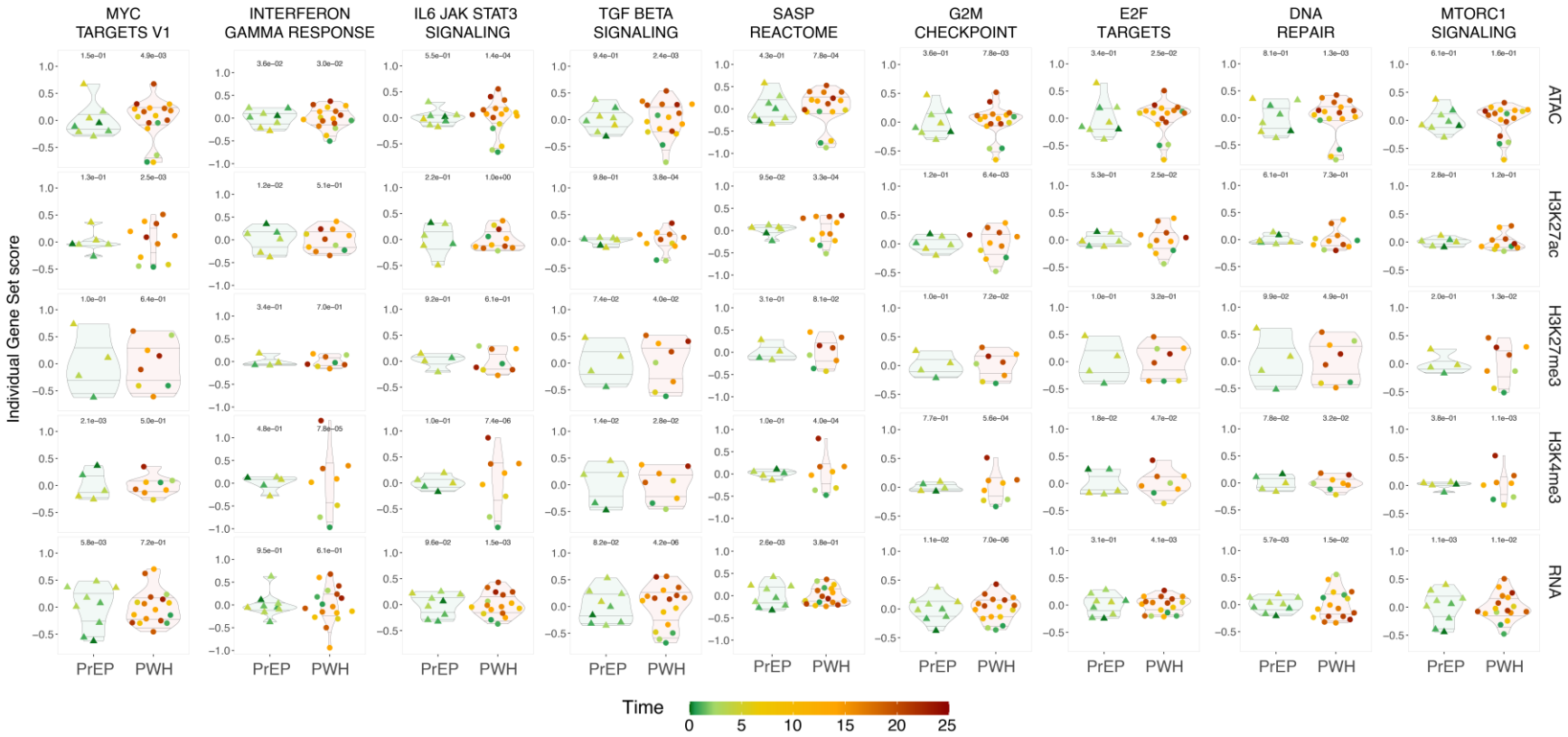

Fig. S4. Per subject GESECA score for eight pathways affected by time as a complement to Fig. 4B.

Each dot represents an individual with colour shading indicating time on ART for PrEP or for PWH. GESECA scores per individual were plotted on the y-axis and subjects were separated by groups on the x-axis. The quantiles are shown as violins for reference of the distribution. A linear model was used to test the correlation of time on ART on PrEP or on PWH with the individual GESECA scores for all tested assays. *P*-values for the correlations are shown at the top of each comparison.

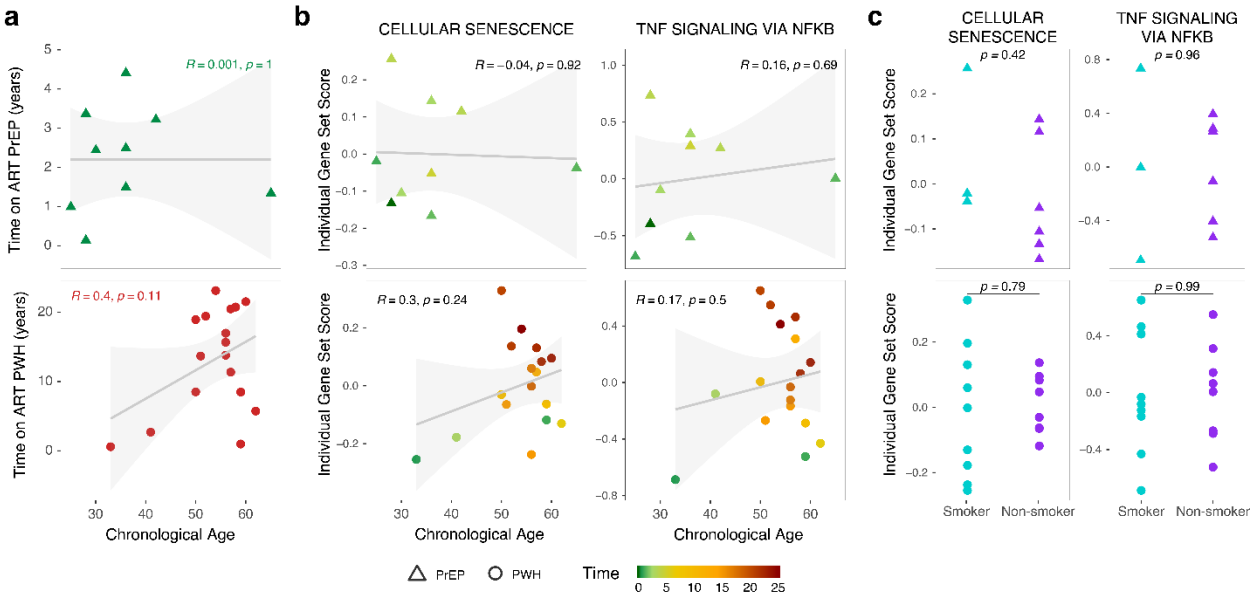

Fig. S5. Effect of chronological age and smoking status on ART associated pathways.

(**a**) Correlation plot between chronological age and time on ART for people on PrEP (top) or for PWH (bottom). (**b**) Correlation plot between individual gene set scores of the RNA assay for two main pathways associated with time and chronological age. (**c**) Comparison of individual gene set scores of the RNA assay and smoking status for two main pathways associated with time on ART. PrEP subjects are shown on top and PWH at the bottom graphs. The *p*-values indicate differences in the mean GESECA scores between groups.

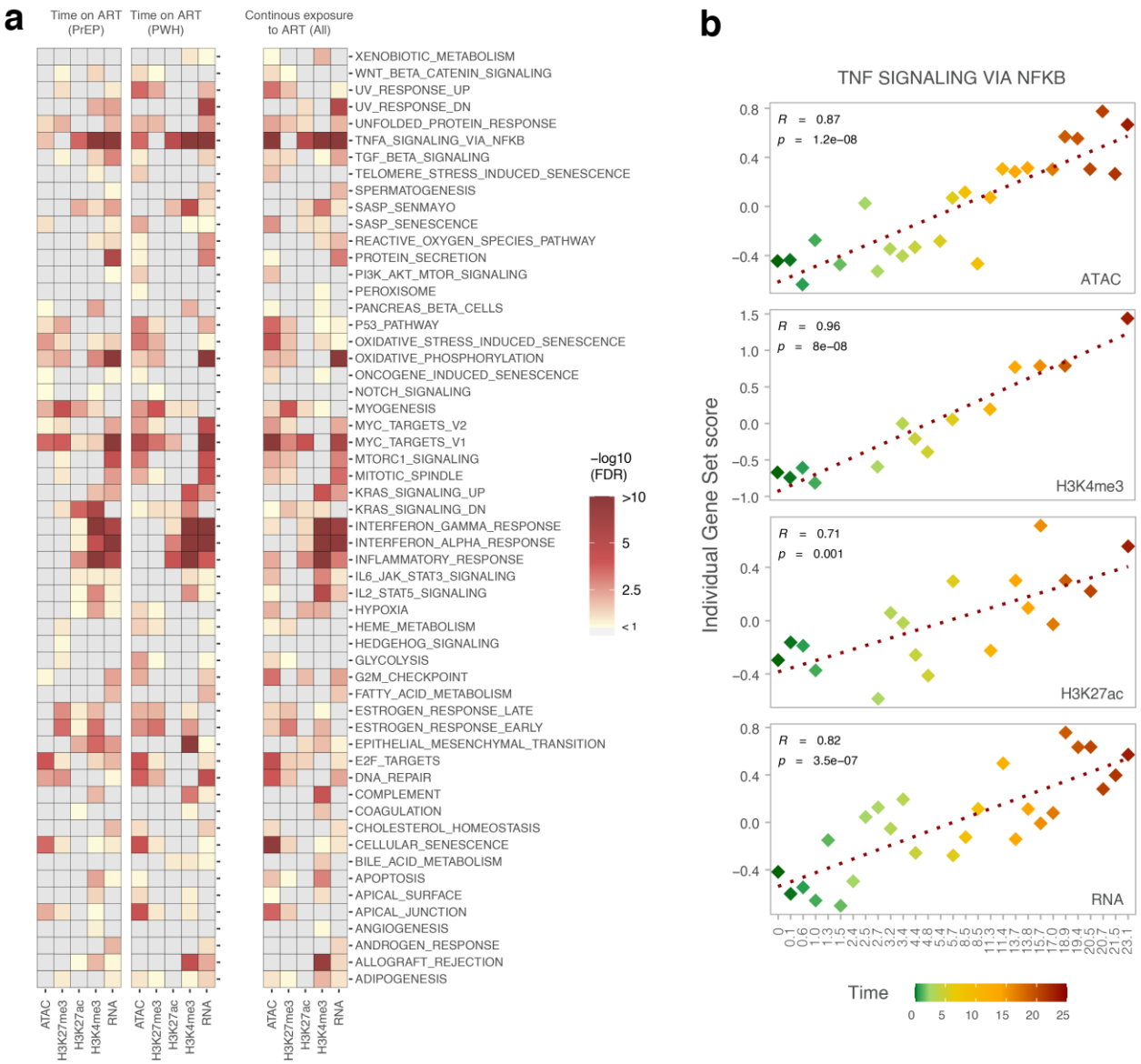

Fig. S6. GESECA association with continuous exposure to.

(**a**) GESECA for Hallmark pathways for time on ART in PrEP (left), in PWH (center), and continuous exposure to ART irrespective of the group (right). FDR for all tested gene sets is shown as a heatmap with increased significance from yellow to red.(**b**) Correlation of individual gene set scores (y-axis) for the TNF signaling pathway with length of ART exposure (x-axis). Pearson correlation R and corresponding *p*-values are shown at the top left of the plots.

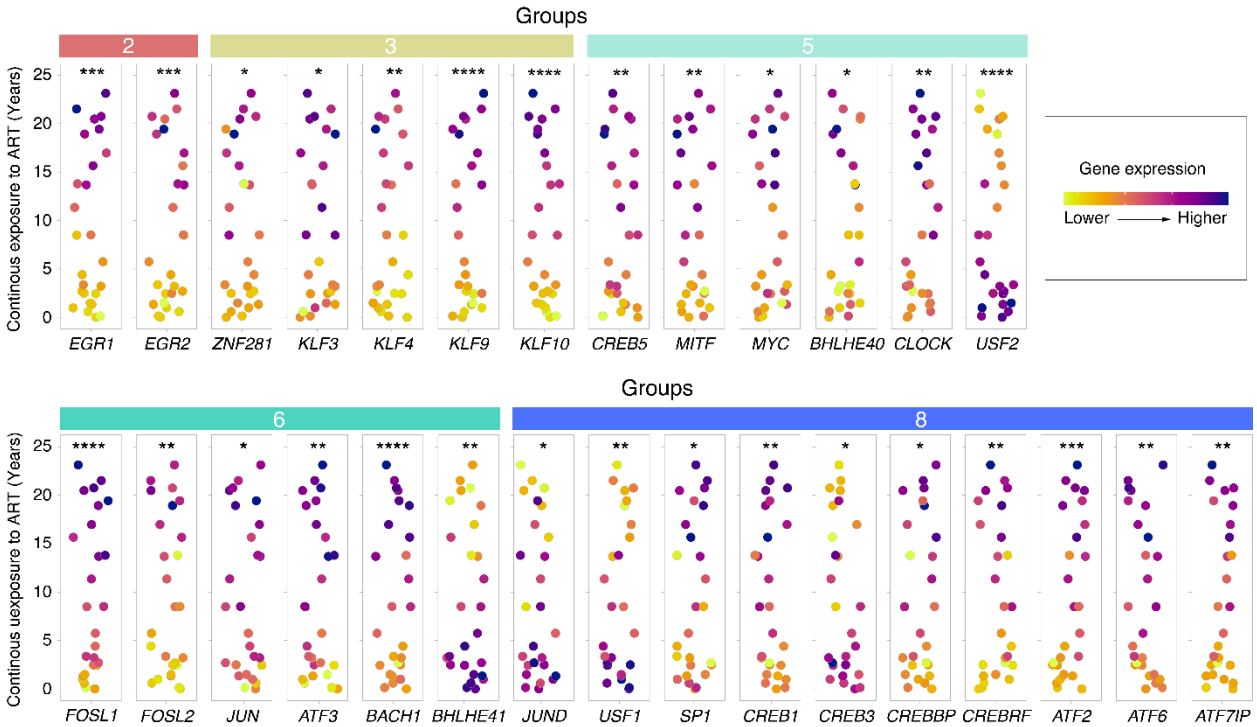

Fig. S7. Coordinated increased gene expression in AM of transcription factors with motifs associated with continuous exposure to ART.

Boxplots showing the time of continuous exposure to ART on the y-axes for genes encoding transcription factors (TF) shown in Fig. 4d. Each dot indicates the continuous exposure to ART for all subjects. The boxes at the top of the plots show the corresponding groups for the TF gene. FDR significance for the continuous exposure to ART. *, FDR < 10%, ** FDR < 1%, *** FDR < 0.1% and, **** FDR < 0.01%.

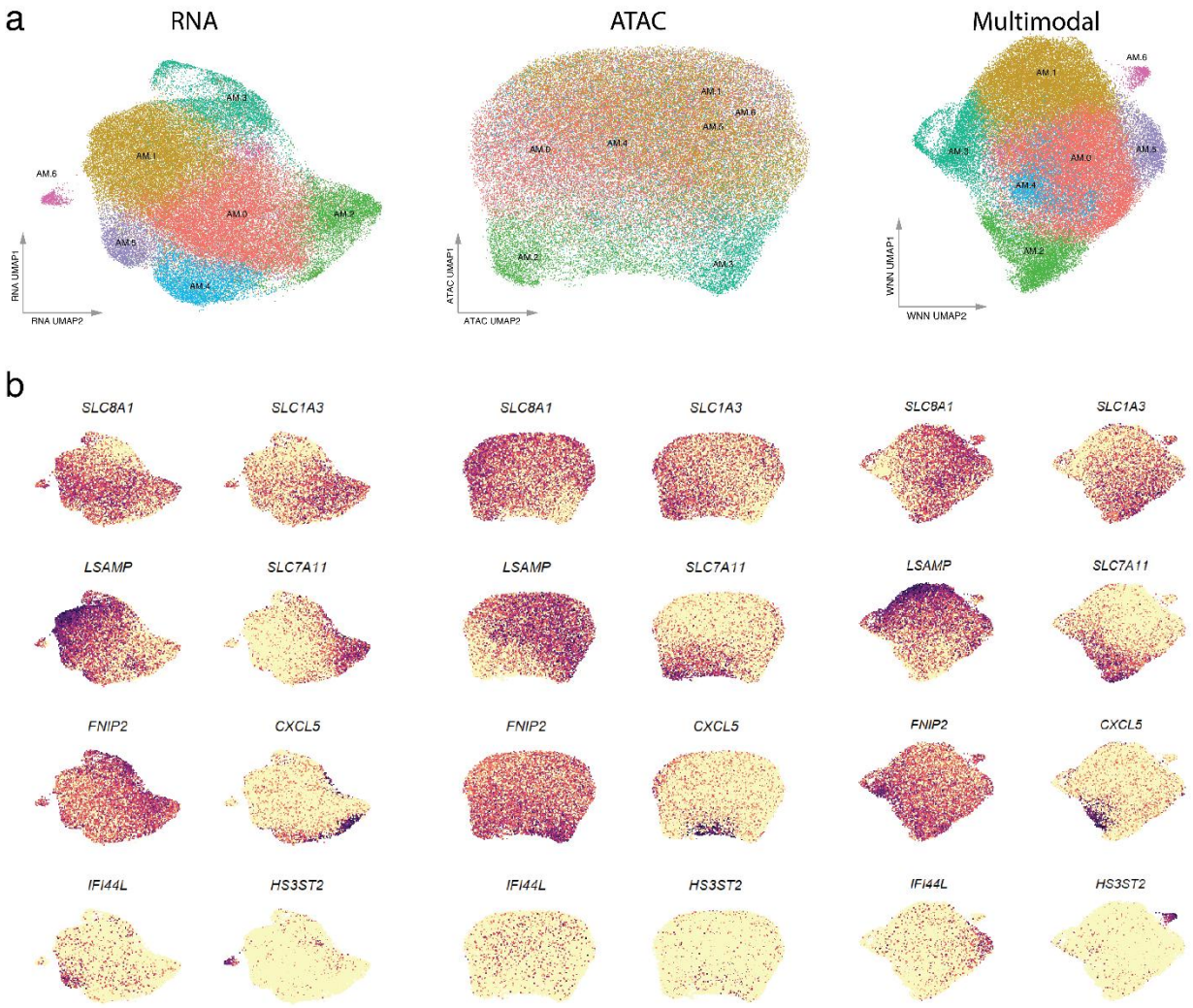

Fig. S8. Annotation of AM subpopulation with single nucleus multiomics.

(a) UMAPs for each modality (RNA and ATAC), as well as the multimodal weighted nearest neighbor (WNN) integration, showing the annotated AM subpopulations defined via single nucleus multimodality. (b) UMAPs displaying the expression of top cluster markers for each AM subpopulation.

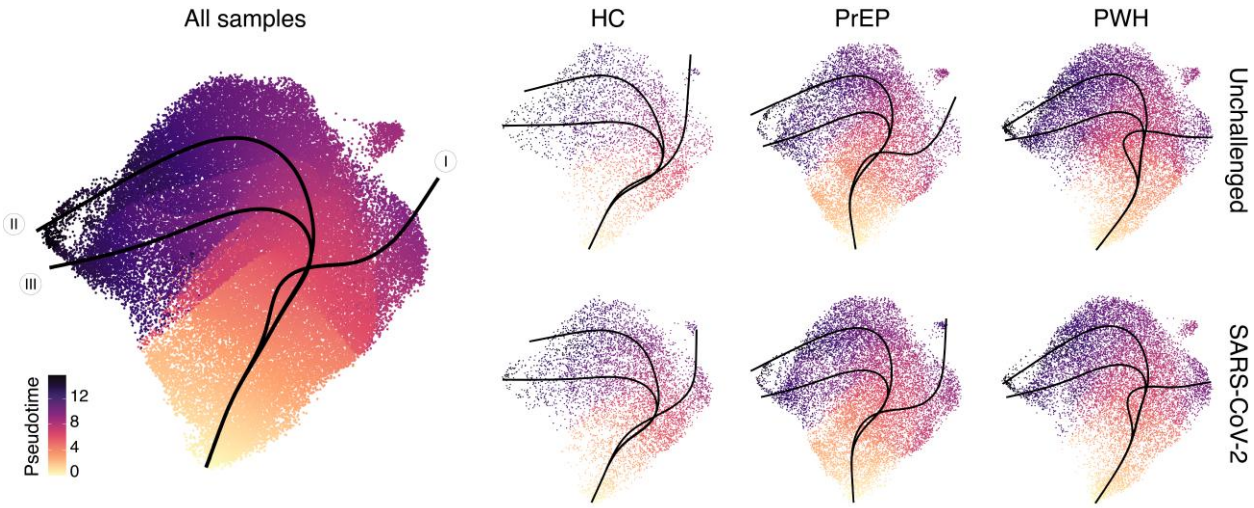

Fig S9. Pseudotime and trajectory analysis.

The starting point of the pseudotime scale and the initial trajectory were obtained unsupervised from the data. Trajectory branches are shown as black lines on top of the UMAP. The left panel shows the trajectory obtained for all cells. The panel on the right shows the trajectory for each group separated by SARS-CoV-2 challenge status.

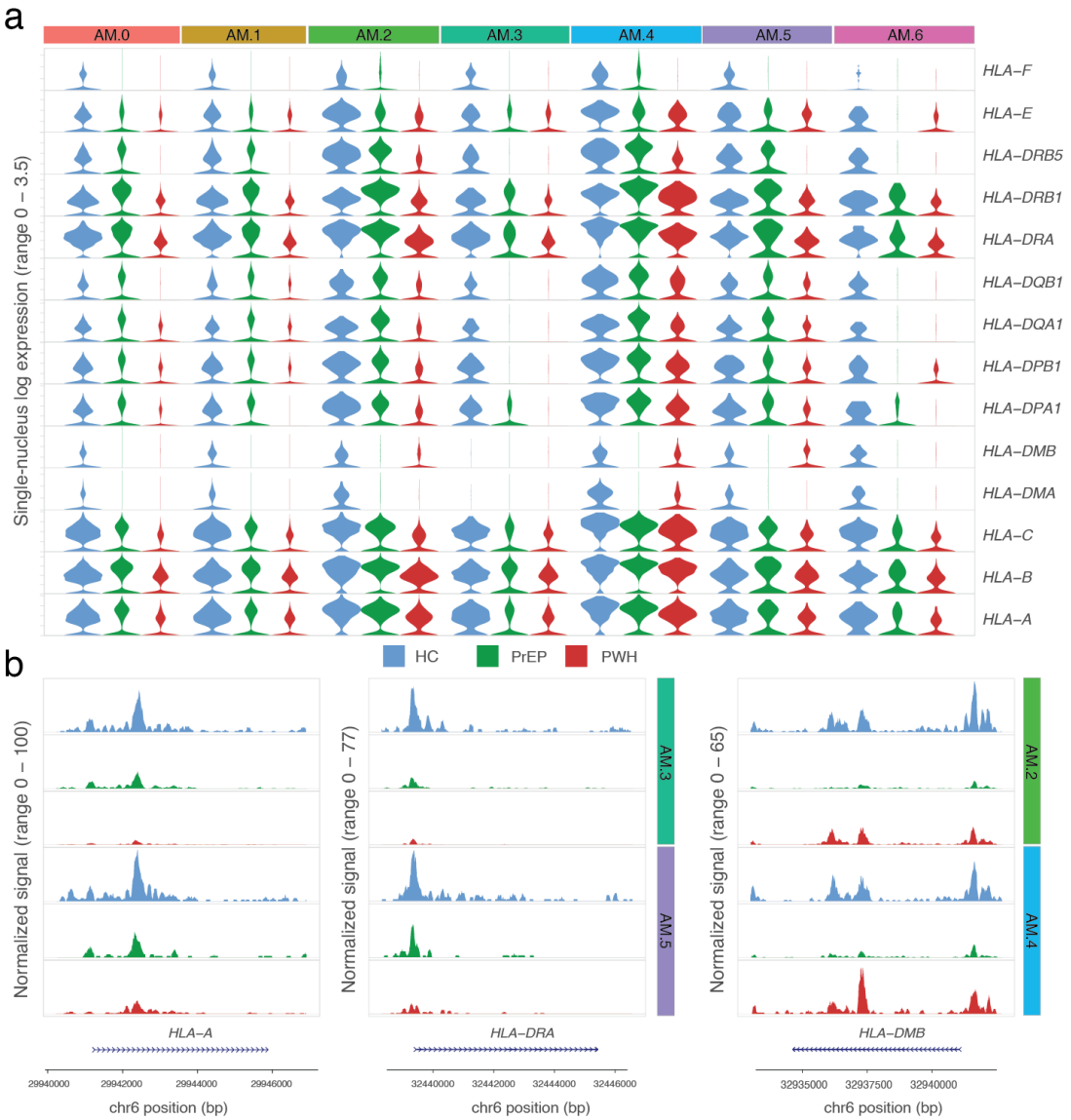

Fig. S10. Constitutive HLA gene expression and chromatin accessibility is impaired in AM from participants on ART.

(a) Single-nucleus expression of HLA genes. Violin plots indicate the per cell expression of the genes listed on the right. (b) Chromatin accessibility plots for the classical class I *HLA-A* and class II *HLA-DRB1* genes in the AM.3 and AM.5 subpopulations and the non-classical class II *HLA-DMB* for AM.2 and AM.4 subpopulations. Tracks display peaks representing baseline chromatin accessibility down sampled to show the same number of cells per group.

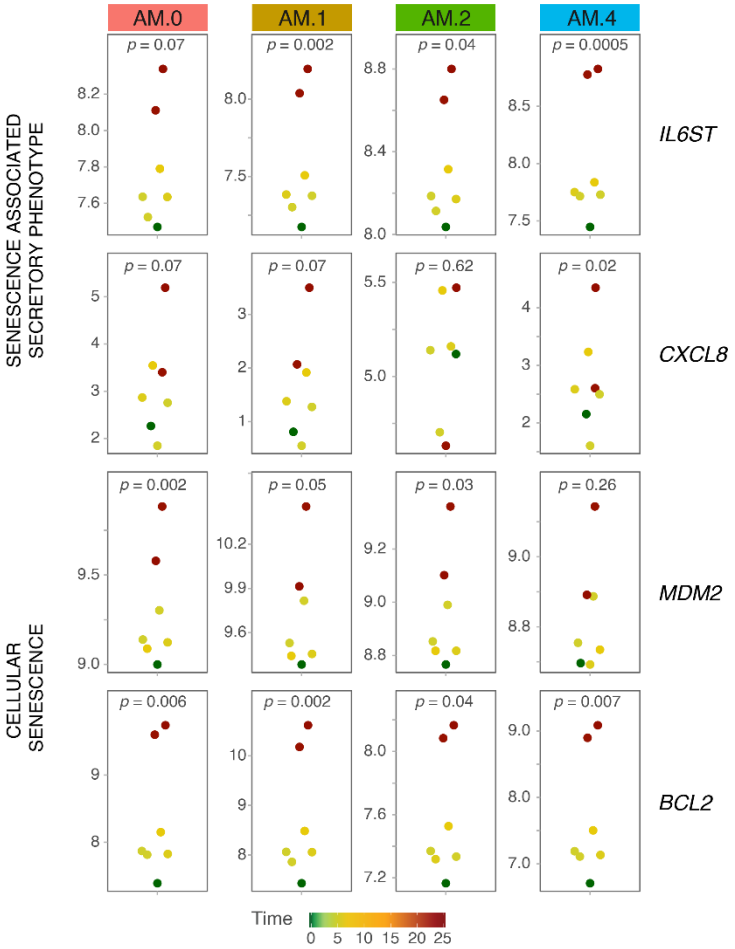

Fig. S11. Senescence markers associate with continuous exposure to ART at the single-nucleus level. Normalized pseudobulk gene expression across timepoints of continuous exposure to ART per AM subpopulation for selected genes from Senescence Associated Secretory Phenotype (SASP) and cellular senescence HALLMARK gene sets.

Reference

1. Tseng A, Seet J, Phillips EJ. The evolution of three decades of antiretroviral therapy: challenges, triumphs and the promise of the future. Br J Clin Pharmacol. 2015;79(2):182-94.
2. Premeaux TA, Ndhlovu LC. Decrypting biological hallmarks of aging in people with HIV. Curr Opin HIV AIDS. 2023;18(5):237-45.
3. Balderson BH, Grothaus L, Harrison RG, McCoy K, Mahoney C, Catz S. Chronic illness burden and quality of life in an aging HIV population. AIDS Care. 2013;25(4):451-8.
4. Nanditha NGA, Paiero A, Tafessu HM, St-Jean M, McLinden T, Justice AC, et al. Excess burden of age-associated comorbidities among people living with HIV in British Columbia, Canada: a population-based cohort study. BMJ open. 2021;11(1):e041734.
5. Chawla A, Wang C, Patton C, Murray M, Punekar Y, de Ruiter A, et al. A Review of Long-Term Toxicity of Antiretroviral Treatment Regimens and Implications for an Aging Population. Infect Dis Ther. 2018;7(2):183-95.
6. Fitzpatrick ME, Kunisaki KM, Morris A. Pulmonary disease in HIV-infected adults in the era of antiretroviral therapy. AIDS. 2018;32(3):277-92.
7. Crothers K, Huang L, Goulet JL, Goetz MB, Brown ST, Rodriguez-Barradas MC, et al. HIV infection and risk for incident pulmonary diseases in the combination antiretroviral therapy era. Am J Respir Crit Care Med. 2011;183(3):388-95.
8. Schoepf IC, Esteban-Cantos A, Thorball CW, Rodes B, Reiss P, Rodriguez-Centeno J, et al. Epigenetic ageing accelerates before antiretroviral therapy and decelerates after viral suppression in people with HIV in Switzerland: a longitudinal study over 17 years. Lancet Healthy Longev. 2023;4(5):e211-e8.
9. Dube M, Tastet O, Dufour C, Sannier G, Brassard N, Delgado GG, et al. Spontaneous HIV expression during suppressive ART is associated with the magnitude and function of HIV-specific CD4(+) and CD8(+) T cells. Cell Host Microbe. 2023;31(9):1507-22 e5.
10. Fastenackels S, Sauce D, Vigouroux C, Avettand-Fenoel V, Bastard JP, Fellahi S, et al. HIV-mediated immune aging in young adults infected perinatally or during childhood. AIDS. 2019;33(11):1705-10.
11. Yang CX, Schon E, Obeidat M, Kobor MS, McEwen L, MacIsaac J, et al. Occurrence of Accelerated Epigenetic Aging and Methylation Disruptions in Human Immunodeficiency Virus Infection Before Antiretroviral Therapy. J Infect Dis. 2021;223(10):1681-9.
12. Corley MJ, Sacdalan C, Pang APS, Chomchey N, Ratnaratorn N, Valcour V, et al. Abrupt and altered cell-type specific DNA methylation profiles in blood during acute HIV infection persists despite prompt initiation of ART. PLoS Pathog. 2021;17(8):e1009785.
13. Bigna JJ, Kenne AM, Asangbeh SL, Sibetcheu AT. Prevalence of chronic obstructive pulmonary disease in the global population with HIV: a systematic review and meta-analysis. Lancet Glob Health. 2018;6(2):e193-e202.
14. Wang Y, Xie Y, Hu S, Ai W, Tao Y, Tang H, et al. Systematic Review and Meta-Analyses of The Interaction Between HIV Infection And COVID-19: Two Years' Evidence Summary. Front Immunol. 2022;13:864838.
15. Bertagnolio S, Thwin SS, Silva R, Nagarajan S, Jassat W, Fowler R, et al. Clinical features of, and risk factors for, severe or fatal COVID-19 among people living with HIV admitted to hospital: analysis of data from the WHO Global Clinical Platform of COVID-19. Lancet HIV. 2022;9(7):e486-e95.
16. WHO. Global tuberculosis report 2023. 2023.

17. Correa-Macedo W, Fava VM, Orlova M, Cassart P, Olivenstein R, Sanz J, et al. Alveolar macrophages from persons living with HIV show impaired epigenetic response to Mycobacterium tuberculosis. J Clin Invest. 2021;131(22).
18. Feikin DR, Feldman C, Schuchat A, Janoff EN. Global strategies to prevent bacterial pneumonia in adults with HIV disease. Lancet Infect Dis. 2004;4(7):445-55.
19. Zifodya JS, Crothers K. Treating bacterial pneumonia in people living with HIV. Expert Rev Respir Med. 2019;13(8):771-86.
20. Maitre T, Cottenet J, Beltramo G, Georges M, Blot M, Piroth L, et al. Increasing burden of noninfectious lung disease in persons living with HIV: a 7-year study using the French nationwide hospital administrative database. Eur Respir J. 2018;52(3).
21. Haas CB, Engels EA, Horner MJ, Freedman ND, Luo Q, Gershman S, et al. Trends and risk of lung cancer among people living with HIV in the USA: a population-based registry linkage study. Lancet HIV. 2022;9(10):e700-e8.
22. Sigel K, Makinson A, Thaler J. Lung cancer in persons with HIV. Curr Opin HIV AIDS. 2017;12(1):31-8.
23. Meyer KC, Raghu G, Baughman RP, Brown KK, Costabel U, du Bois RM, et al. An official American Thoracic Society clinical practice guideline: the clinical utility of bronchoalveolar lavage cellular analysis in interstitial lung disease. Am J Respir Crit Care Med. 2012;185(9):1004-14.
24. Parks B, Greenleaf W. Scalable high-performance single cell data analysis with BPCells. bioRxiv. 2025:2025.03.27.645853.
25. Hao Y, Stuart T, Kowalski MH, Choudhary S, Hoffman P, Hartman A, et al. Dictionary learning for integrative, multimodal and scalable single-cell analysis. Nature biotechnology. 2024;42(2):293-304.
26. Stuart T, Srivastava A, Madad S, Lareau CA, Satija R. Single-cell chromatin state analysis with Signac. Nature methods. 2021;18(11):1333-41.
27. Yu G, Wang LG, Han Y, He QY. clusterProfiler: an R package for comparing biological themes among gene clusters. OMICS. 2012;16(5):284-7.
28. Alquicira-Hernandez J, Powell JE. Nebulosa recovers single-cell gene expression signals by kernel density estimation. Bioinformatics. 2021;37(16):2485-7.
29. Street K, Risso D, Fletcher RB, Das D, Ngai J, Yosef N, et al. Slingshot: cell lineage and pseudotime inference for single-cell transcriptomics. BMC genomics. 2018;19(1):477.
30. Murall CL, Fournier E, Galvez JH, N'Guessan A, Reiling SJ, Quirion PO, et al. A small number of early introductions seeded widespread transmission of SARS-CoV-2 in Quebec, Canada. Genome Med. 2021;13(1):169.
31. Ritchie ME, Phipson B, Wu D, Hu Y, Law CW, Shi W, et al. limma powers differential expression analyses for RNA-sequencing and microarray studies. Nucleic Acids Res. 2015;43(7):e47.
32. Law CW, Chen Y, Shi W, Smyth GK. voom: Precision weights unlock linear model analysis tools for RNA-seq read counts. Genome Biol. 2014;15(2):R29.
33. Robinson MD, McCarthy DJ, Smyth GK. edgeR: a Bioconductor package for differential expression analysis of digital gene expression data. Bioinformatics. 2010;26(1):139-40.
34. Yu G, Wang LG, He QY. ChIPseeker: an R/Bioconductor package for ChIP peak annotation, comparison and visualization. Bioinformatics. 2015;31(14):2382-3.
35. Sergushichev AA. An algorithm for fast preranked gene set enrichment analysis using cumulative statistic calculation. bioRxiv. 2016:060012.

36. Liberzon A, Birger C, Thorvaldsdottir H, Ghandi M, Mesirov JP, Tamayo P. The Molecular Signatures Database (MSigDB) hallmark gene set collection. Cell Syst. 2015;1(6):417-25.
37. Milacic M, Beavers D, Conley P, Gong C, Gillespie M, Griss J, et al. The Reactome Pathway Knowledgebase 2024. Nucleic Acids Res. 2024;52(D1):D672-D8.
38. Saul D, Kosinsky RL, Atkinson EJ, Doolittle ML, Zhang X, LeBrasseur NK, et al. A new gene set identifies senescent cells and predicts senescence-associated pathways across tissues. Nature communications. 2022;13(1):4827.
39. Heinz S, Benner C, Spann N, Bertolino E, Lin YC, Laslo P, et al. Simple combinations of lineage-determining transcription factors prime cis-regulatory elements required for macrophage and B cell identities. Molecular cell. 2010;38(4):576-89.
40. Mahony S, Auron PE, Benos PV. DNA familial binding profiles made easy: comparison of various motif alignment and clustering strategies. PLoS Comput Biol. 2007;3(3):e61.
41. Bentsen M, Goymann P, Schultheis H, Klee K, Petrova A, Wiegandt R, et al. ATAC-seq footprinting unravels kinetics of transcription factor binding during zygotic genome activation. Nature communications. 2020;11(1):4267.
42. Zou J, Ernst J. Chromatin state modeling across individuals reveals global patterns of histone modifications. bioRxiv. 2022:2022.08.02.502571.
43. Grubert F, Zaugg JB, Kasowski M, Ursu O, Spacek DV, Martin AR, et al. Genetic Control of Chromatin States in Humans Involves Local and Distal Chromosomal Interactions. Cell. 2015;162(5):1051-65.
44. Ramirez F, Ryan DP, Gruning B, Bhardwaj V, Kilpert F, Richter AS, et al. deepTools2: a next generation web server for deep-sequencing data analysis. Nucleic Acids Res. 2016;44(W1):W160-5.
45. Rauluseviciute I, Riudavets-Puig R, Blanc-Mathieu R, Castro-Mondragon JA, Ferenc K, Kumar V, et al. JASPAR 2024: 20th anniversary of the open-access database of transcription factor binding profiles. Nucleic Acids Res. 2024;52(D1):D174-D82.
46. Wickham H. ggplot2: Elegant Graphics for Data Analysis: Springer Publishing Company, Incorporated; 2009. 216 p.
47. Kaplan D, Pruim R. ggformula: Formula Interface to the Grammar of Graphics. https://githubcom/ProjectMOSAIC/ggformula. 2023.
48. Badia IMP, Velez Santiago J, Braunger J, Geiss C, Dimitrov D, Muller-Dott S, et al. decoupleR: ensemble of computational methods to infer biological activities from omics data. Bioinform Adv. 2022;2(1):vbac016.
49. Dallmann-Sauer M, Fava VM, Malherbe ST, MacDonald CE, Orlova M, Kroon EE, et al. Mycobacterium tuberculosis resisters despite HIV exhibit activated T cells and macrophages in their pulmonary alveoli. J Clin Invest. 2025;135(7).
50. Fleck JS, Jansen SMJ, Wollny D, Zenk F, Seimiya M, Jain A, et al. Inferring and perturbing cell fate regulomes in human brain organoids. Nature. 2023;621(7978):365-72.
51. Fornes O, Castro-Mondragon JA, Khan A, van der Lee R, Zhang X, Richmond PA, et al. JASPAR 2020: update of the open-access database of transcription factor binding profiles. Nucleic Acids Res. 2020;48(D1):D87-D92.
52. Charrier-Savournin FB, Chateau MT, Gire V, Sedivy J, Piette J, Dulic V. p21-Mediated nuclear retention of cyclin B1-Cdk1 in response to genotoxic stress. Mol Biol Cell. 2004;15(9):3965-76.

53. Wang XW, Zhan Q, Coursen JD, Khan MA, Kontny HU, Yu L, et al. GADD45 induction of a G2/M cell cycle checkpoint. Proc Natl Acad Sci U S A. 1999;96(7):3706-11.
54. Zannini L, Delia D, Buscemi G. CHK2 kinase in the DNA damage response and beyond. J Mol Cell Biol. 2014;6(6):442-57.
55. Acosta JC, Banito A, Wuestefeld T, Georgilis A, Janich P, Morton JP, et al. A complex secretory program orchestrated by the inflammasome controls paracrine senescence. Nat Cell Biol. 2013;15(8):978-90.
56. Vadaq N, van de Wijer L, van Eekeren LE, Koenen H, de Mast Q, Joosten LAB, et al. Targeted plasma proteomics reveals upregulation of distinct inflammatory pathways in people living with HIV. iScience. 2022;25(10):105089.
57. Ellwanger JH, Valverde-Villegas JM, Kaminski VL, de Medeiros RM, Almeida SEM, Santos BR, et al. Increased IL-8 levels in HIV-infected individuals who initiated ART with CD4(+) T cell counts <350 cells/mm(3) - A potential hallmark of chronic inflammation. Microbes Infect. 2020;22(9):474-80.
58. Cohen J, D'Agostino L, Wilson J, Tuzer F, Torres C. Astrocyte Senescence and Metabolic Changes in Response to HIV Antiretroviral Therapy Drugs. Front Aging Neurosci. 2017;9:281.
59. Konstantinidis I, Crothers K, Kunisaki KM, Drummond MB, Benfield T, Zar HJ, et al. HIV-associated lung disease. Nat Rev Dis Primers. 2023;9(1):39.
60. Coghill AE, Han X, Suneja G, Lin CC, Jemal A, Shiels MS. Advanced stage at diagnosis and elevated mortality among US patients with cancer infected with HIV in the National Cancer Data Base. Cancer. 2019;125(16):2868-76.
61. Ucero AC, Bakiri L, Roediger B, Suzuki M, Jimenez M, Mandal P, et al. Fra-2-expressing macrophages promote lung fibrosis in mice. J Clin Invest. 2019;129(8):3293-309.
62. Birnhuber A, Biasin V, Schnoegl D, Marsh LM, Kwapiszewska G. Transcription factor Fra-2 and its emerging role in matrix deposition, proliferation and inflammation in chronic lung diseases. Cell Signal. 2019;64:109408.
63. Rincon M, Irvin CG. Role of IL-6 in asthma and other inflammatory pulmonary diseases. Int J Biol Sci. 2012;8(9):1281-90.
64. Liu F, Zhang X, Du W, Du J, Chi Y, Sun B, et al. Diagnosis values of IL-6 and IL-8 levels in serum and bronchoalveolar lavage fluid for invasive pulmonary aspergillosis in chronic obstructive pulmonary disease. J Investig Med. 2021;69(7):1344-9.
65. Chang YP, Tsai YH, Chen YM, Huang KT, Lee CP, Hsu PY, et al. Upregulated microRNA-125b-5p in patients with asthma-COPD overlap mediates oxidative stress and late apoptosis via targeting IL6R/TRIAP1 signaling. Respir Res. 2024;25(1):64.
66. Lopez-Otin C, Blasco MA, Partridge L, Serrano M, Kroemer G. Hallmarks of aging: An expanding universe. Cell. 2023;186(2):243-78.
67. Barnes PJ. Oxidative stress-based therapeutics in COPD. Redox Biol. 2020;33:101544.
68. Casanova-Acebes M, Dalla E, Leader AM, LeBerichel J, Nikolic J, Morales BM, et al. Tissue-resident macrophages provide a pro-tumorigenic niche to early NSCLC cells. Nature. 2021;595(7868):578-84.
69. Dayanc B, Eris S, Gulfirat NE, Ozden-Yilmaz G, Cakiroglu E, Coskun Deniz OS, et al. Integrative multi-omics identifies AP-1 transcription factor as a targetable mediator of acquired osimertinib resistance in non-small cell lung cancer. Cell Death Dis. 2025;16(1):414.
70. Hou H, Sun D, Zhang X. The role of MDM2 amplification and overexpression in therapeutic resistance of malignant tumors. Cancer Cell Int. 2019;19:216.

71. Zong D, Gu J, Cavalcante GC, Yao W, Zhang G, Wang S, et al. BRD4 Levels Determine the Response of Human Lung Cancer Cells to BET Degraders That Potently Induce Apoptosis through Suppression of Mcl-1. Cancer Res. 2020;80(11):2380-93.
72. Alexandrova Y, Costiniuk CT, Jenabian MA. Pulmonary Immune Dysregulation and Viral Persistence During HIV Infection. Front Immunol. 2021;12:808722.
73. Wang Z, Li S, Huang B. Alveolar macrophages: Achilles' heel of SARS-CoV-2 infection. Signal Transduct Target Ther. 2022;7(1):242.
74. Bain CC, Lucas CD, Rossi AG. Pulmonary macrophages and SARS-Cov2 infection. Int Rev Cell Mol Biol. 2022;367:1-28.
75. Magnen M, You R, Rao AA, Davis RT, Rodriguez L, Bernard O, et al. Immediate myeloid depot for SARS-CoV-2 in the human lung. Sci Adv. 2024;10(31):eadm8836.
76. Kotov DI, Lee OV, Fattinger SA, Langner CA, Guillen JV, Peters JM, et al. Early cellular mechanisms of type I interferon-driven susceptibility to tuberculosis. Cell. 2023;186(25):5536-53 e22.
77. Bastard P, Rosen LB, Zhang Q, Michailidis E, Hoffmann HH, Zhang Y, et al. Autoantibodies against type I IFNs in patients with life-threatening COVID-19. Science. 2020;370(6515).
78. Philippot Q, Fekkar A, Gervais A, Le Voyer T, Boers LS, Conil C, et al. Autoantibodies Neutralizing Type I IFNs in the Bronchoalveolar Lavage of at Least 10% of Patients During Life-Threatening COVID-19 Pneumonia. J Clin Immunol. 2023;43(6):1093-103.
79. Pilkington V, Hill A, Hughes S, Nwokolo N, Pozniak A. How safe is TDF/FTC as PrEP? A systematic review and meta-analysis of the risk of adverse events in 13 randomised trials of PrEP. J Virus Erad. 2018;4(4):215-24.
80. Cohen MS, Chen YQ, McCauley M, Gamble T, Hosseinipour MC, Kumarasamy N, et al. Antiretroviral Therapy for the Prevention of HIV-1 Transmission. N Engl J Med. 2016;375(9):830-9.
81. Marrazzo J, Tao L, Becker M, Leech AA, Taylor AW, Ussery F, et al. HIV Preexposure Prophylaxis With Emtricitabine and Tenofovir Disoproxil Fumarate Among Cisgender Women. JAMA. 2024;331(11):930-7.
82. Cox SN, Wu L, Wittenauer R, Clark S, Roberts DA, Nwogu IB, et al. Impact of HIV self-testing for oral pre-exposure prophylaxis scale-up on drug resistance and HIV outcomes in western Kenya: a modelling study. Lancet HIV. 2024;11(3):e167-e75.
83. Choopanya K, Martin M, Suntharasamai P, Sangkum U, Mock PA, Leethochawalit M, et al. Antiretroviral prophylaxis for HIV infection in injecting drug users in Bangkok, Thailand (the Bangkok Tenofovir Study): a randomised, double-blind, placebo-controlled phase 3 trial. Lancet. 2013;381(9883):2083-90.
84. Baeten JM, Donnell D, Ndase P, Mugo NR, Campbell JD, Wangisi J, et al. Antiretroviral prophylaxis for HIV prevention in heterosexual men and women. N Engl J Med. 2012;367(5):399-410.
85. Jourdain H, de Gage SB, Desplas D, Dray-Spira R. Real-world effectiveness of pre-exposure prophylaxis in men at high risk of HIV infection in France: a nested case-control study. Lancet Public Health. 2022;7(6):e529-e36.
86. Hughes SM, Levy CN, Calienes FL, Stekler JD, Pandey U, Vojtech L, et al. Treatment with Commonly Used Antiretroviral Drugs Induces a Type I/III Interferon Signature in the Gut in the Absence of HIV Infection. Cell Rep Med. 2020;1(6):100096.

87. Bowman ER, Cameron C, Richardson B, Kulkarni M, Gabriel J, Kettelhut A, et al. In Vitro Exposure of Leukocytes to HIV Preexposure Prophylaxis Decreases Mitochondrial Function and Alters Gene Expression Profiles. Antimicrob Agents Chemother. 2020;65(1).
88. Cohen J, D'Agostino L, Tuzer F, Torres C. HIV antiretroviral therapy drugs induce premature senescence and altered physiology in HUVECs. Mech Ageing Dev. 2018;175:74-82.
89. Wallace J, Gonzalez H, Rajan R, Narasipura SD, Virdi AK, Olali AZ, et al. Anti-HIV Drugs Cause Mitochondrial Dysfunction in Monocyte-Derived Macrophages. Antimicrob Agents Chemother. 2022;66(4):e0194121.
90. Leeansyah E, Cameron PU, Solomon A, Tennakoon S, Velayudham P, Gouillou M, et al. Inhibition of telomerase activity by human immunodeficiency virus (HIV) nucleos(t)ide reverse transcriptase inhibitors: a potential factor contributing to HIV-associated accelerated aging. J Infect Dis. 2013;207(7):1157-65.
91. Kim S, Lee SA, Yoon H, Kim MY, Yoo JK, Ahn SH, et al. Exosome-based delivery of super-repressor IkappaBalpha ameliorates kidney ischemia-reperfusion injury. Kidney Int. 2021;100(3):570-84.
92. Park YJ, Bae J, Yoo JK, Ahn SH, Park SY, Kim YS, et al. Effects of NF-kappaB Inhibitor on Sepsis Depend on the Severity and Phase of the Animal Sepsis Model. J Pers Med. 2024;14(6).
93. Lee CJ, Jang SH, Lim J, Park H, Ahn SH, Park SY, et al. Exosome-based targeted delivery of NF-kappaB ameliorates age-related neuroinflammation in the aged mouse brain. Exp Mol Med. 2025;57(1):235-48.
94. Yuan X, Ruan W, Bobrow B, Carmeliet P, Eltzschig HK. Targeting hypoxia-inducible factors: therapeutic opportunities and challenges. Nat Rev Drug Discov. 2024;23(3):175-200.
95. Bui BP, Nguyen PL, Lee K, Cho J. Hypoxia-Inducible Factor-1: A Novel Therapeutic Target for the Management of Cancer, Drug Resistance, and Cancer-Related Pain. Cancers (Basel). 2022;14(24).
96. Wicks EE, Semenza GL. Hypoxia-inducible factors: cancer progression and clinical translation. J Clin Invest. 2022;132(11).
97. Chaib S, Tchkonia T, Kirkland JL. Cellular senescence and senolytics: the path to the clinic. Nat Med. 2022;28(8):1556-68.
98. Mannarino M, Cherif H, Ghazizadeh S, Martinez OW, Sheng K, Cousineau E, et al. Senolytic treatment for low back pain. Sci Adv. 2025;11(11):eadr1719.
99. Rivera CG, Zeuli JD, Smith BL, Johnson TM, Bhatia R, Otto AO, et al. HIV Pre-Exposure Prophylaxis: New and Upcoming Drugs to Address the HIV Epidemic. Drugs. 2023;83(18):1677-98.
100. Landovitz RJ, Donnell D, Clement ME, Hanscom B, Cottle L, Coelho L, et al. Cabotegravir for HIV Prevention in Cisgender Men and Transgender Women. N Engl J Med. 2021;385(7):595-608.
101. Delany-Moretlwe S, Hughes JP, Bock P, Ouma SG, Hunidzarira P, Kalonji D, et al. Cabotegravir for the prevention of HIV-1 in women: results from HPTN 084, a phase 3, randomised clinical trial. Lancet. 2022;399(10337):1779-89.
102. Marrazzo J. Lenacapavir for HIV-1 - Potential Promise of a Long-Acting Antiretroviral Drug. N Engl J Med. 2022;386(19):1848-9.